

Predictive dynamical modeling and stability of the equilibria in a discrete fractional difference COVID-19 epidemic model

Yu-Ming Chu ^a, Saima Rashid ^{b,*}, Ahmet Ocak Akdemir ^c, Aasma Khalid ^d, Dumitru Baleanu ^{e,f,g,*}, Bushra R. Al-Sinan ^h, O.A.I. Elzibar ⁱ

^a Department of Mathematics, Huzhou University, Huzhou, 313000, China

^b Department of Mathematics, Government College University, Faisalabad 38000, Pakistan

^c Department of Mathematics, Faculty of Science and Arts, Agri Ibrahim Cecen University, Agri, Turkey

^d Department of Mathematics, Government College women University, Faisalabad, Pakistan

^e Department of Mathematics, Cankaya University, Ankara, Turkey

^f Institute of Space Sciences, 06530 Bucharest, Romania

^g Department of Natural Sciences, School of Arts and Sciences, Lebanese American University, Beirut 11022801, Lebanon

^h University of Hafr Al-Batin, Nairiyah College, Department of Administrative and Financial Sciences, Saudi Arabia

ⁱ Department of Mathematics, Turabah University College, Taif University, P.O. Box 1109, Taif 21944, Saudi Arabia

ARTICLE INFO

MSC:

26A51

26A33

26D07

26D10

26D15

Keywords:

Fractional difference equation

Discrete fractional operator

Equilibrium points

Local and global stability

Existence and uniqueness

ABSTRACT

The SARSCoV-2 virus, also known as the coronavirus-2, is the consequence of COVID-19, a severe acute respiratory syndrome. Droplets from an infectious individual are how the pathogen is transmitted from one individual to another and occasionally, these particles can contain toxic textures that could also serve as an entry point for the pathogen. We formed a discrete fractional-order COVID-19 framework for this investigation using information and inferences from Thailand. To combat the illnesses, the region has implemented mandatory vaccination, interpersonal stratification and mask distribution programs. As a result, we divided the vulnerable people into two groups: those who support the initiatives and those who do not take the influence regulations seriously. We analyze endemic problems and common data while demonstrating the threshold evolution defined by the fundamental reproductive quantity \mathbb{R}_0 . Employing the mean general interval, we have evaluated the configuration value systems in our framework. Such a framework has been shown to be adaptable to changing pathogen populations over time. The Picard Lindelöf technique is applied to determine the existence-uniqueness of the solution for the proposed scheme. In light of the relationship between the \mathbb{R}_0 and the consistency of the fixed points in this framework, several theoretical conclusions are made. Numerous numerical simulations are conducted to validate the outcome.

Introduction

Coronavirus disease 2019 (COVID-19) is a severe respiratory pathogen brought on by an infestation with the SARS-CoV-2 virus. The approved identity was awarded by the World Health Organization (WHO), which defined it as CO for corona, VI for virus, D for disease, and 19 representing the year of determination. The clinical manifestations of an infection include the flu, a persistent cough, exhaustion, a stomachache and breathing problems. On December 8, 2019, in Wuhan, Republic of China, COVID-19 was first identified and characterized. On March 11, 2020, WHO designated COVID-19 as a disease outbreak due to the infectious agent's quick propagation to other states and continents. Coronavirus typically results in either

virus-or bacteria-related pneumonia, whether explicitly or implicitly. There are numerous discrepancies regarding the provenance of the 2019 coronavirus (COVID-19), despite the widespread conviction that it is a viral vector inferred from bats. In this situation, the very first concern that needs to be addressed relates to whether or not bats are native to the entire planet; if they are, then why has not this outbreak started previously? Why did not that pathogen infect humans sooner? According to one hypothesis, the ailment was transmitted to individuals by Chinese people consuming unpasteurized bats. It would have been wonderful to get out and return to some of the African villages in which individuals still eat junk food that has been mauled by bats. If this theory is accurate, bats may be able to spread this illness. Given that

* Corresponding authors.

E-mail addresses: chuyuming@zjhu.edu.cn (Y.-M. Chu), saimarashid@gcu.edu.pk (S. Rashid), ahmetakdemir@agri.edu.tr (A.O. Akdemir), aasmakhalid@gcuwf.edu.com (A. Khalid), dumitru@cankaya.edu.tr (D. Baleanu), Bushra@uhb.edu.sa (B.R. Al-Sinan), Oazibar@tu.edu.sa (O.A.I. Elzibar).

<https://doi.org/10.1016/j.rinp.2023.106467>

Received 12 March 2023; Received in revised form 13 April 2023; Accepted 17 April 2023

Available online 28 April 2023

2211-3797/© 2023 The Authors. Published by Elsevier B.V. This is an open access article under the CC BY-NC-ND license (<http://creativecommons.org/licenses/by-nc-nd/4.0/>).

bats are a major ingredient in the local regimen, there is a chance that residents could contract the viral infection from other people. A variety of magazines were released in 1981, “The Eyes of Darkness” being one of them. This novel depicts the virus outbreak, or how it would start. In addition, the pathogen is described in this book as a bioweapon. “The End of the World Book”, another novel, states very clearly when the virus outbreak started.

By expressing the most probable consequence of an outbreak, differential equations (DEs) can assist interventions in improving the general population’s health. The reviewers summarized the concept of scientific methods in epidemiological studies for genetic conditions such as HIV/AIDS, rhinoviruses, chikungunya, hantavirus and others in [1]. The influence of specific instances of specialized treatment and its repercussions on lessening cholera propagation were researched in [2]. In an additional investigation [3], therapies were administered to those who were at risk in an effort to stop the dissemination of the Ebola virus. In [4], unconventional methods for addressing the dynamical DE systems of the physically based infectious disease configurations were designed using the reproducing kernel scheme. Numerous algorithms have also been applied to determine the complexities of COVID-19 in [5]. Three numerical strategies were used to scrutinize the COVID-19 complexities in [6,7] utilizing the methodologies of power and general kernel fractional operators. The researchers developed a framework in [8] that combined the signifiers taken from the Wuhan infestation (China). The idea of numerical simulations was used in [9] to analyze the COVID-19 evolution in Italy. The investigation [10] described a fractional, nearly incompressible framework for the propagation of COVID-19 using Louisiana State documents in the United States. In [11], a numerical framework was employed to examine the modeling of COVID-19 dissemination in a northeast Brazilian region. In the task [12], a proposed form of COVID-19 was investigated utilizing stability hypotheses for DEs alongside real-world documentation from Pakistan. In [13], a modified Adams–Bashforth mechanism was implemented to rectify an innovative design of COVID-19 that was properly considered by substituting a fractional formulation with a Mittag-Leffler kernel for the ordinary derivatives. In accordance with the findings in [14], evolutionary computation could significantly lower the propagation and mortality rates of COVID-19 in Ghana. Furthermore, using a fractional framework for the lock-down component, the authors investigated the lock-down impact on COVID-19 propagation in Turkey [15]. Hermite wavelets were applied to study the fractional COVID-19 methodology developed in [16], and the outcomes were evaluated by comparing them to those obtained employing the Adams–Bashforth–Moulton predictor–corrector procedure. Safare et al. [17] used a collection of actual statistics to broaden the COVID-19 framework while accounting for the effects of detachment and phytosanitary. Lévy jump disturbances and white noise were incorporated into all design components, and the random walk solvent close to the computational governing equations was utilized to investigate the dynamic systems’ stochastic features in [18], which also presented and analyzed a stochastic COVID-19 framework for Lévy noise. A subsequent study [19] used a fractional intensity adaptable Fourier structure to test the COVID-19 controllability alongside multidimensional developments and fractional interconnection. Non-pharmaceutical initiatives that relied on mathematical data analysis were first invented to combat COVID-19 in [20], and the threshold requirements for infection-free equilibrium were investigated. Koufi and Koufi [21] investigated the use of non-standard estimations to analyze the dynamical disease outbreak framework of COVID-19 based on parameterized nonlinearities and associated uncertainties. The document [22] furthermore glanced at the COVID-19 approach for bats, presenters, reservoirs and individuals and employed the variational iteration procedure to arrive at an approximation of its solution. Thailand has implemented precautions for individuals to secure themselves by donning respirators, staying away from crowded areas, sanitizing their hands frequently, and being encouraged to use alcohol gel to

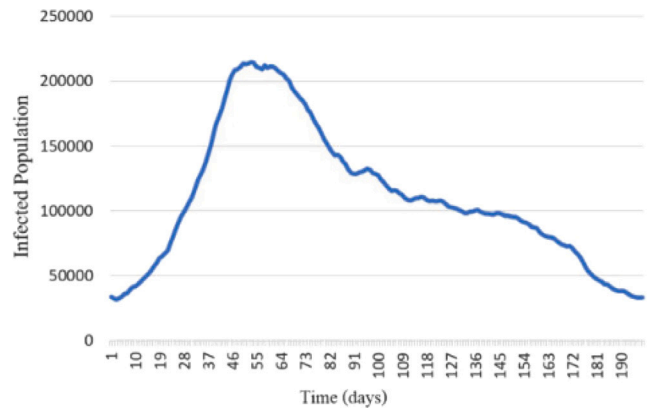


Fig. 1. Highly infectious individuals from June to December 2021 (see; [23]).

cease the transmission of the virus. Because there are only so many therapies available, the public health presidency expanded vaccination programs for the elderly and those at risk. This is because treatments are essential in the struggle against COVID-19 pathogens. The Sinovac vaccine, which is the paramount vaccination, has been supplied in Thailand in conjunction with the AstraZeneca/Oxford vaccine. Numerous different pharmaceuticals like Johnson & Johnson, Moderna, and Pfizer/BioNTech were not extensively utilized because individuals were not readily available; however, they are presently available. The number of reported affected individuals in Thailand from June to December 2021 is depicted in Fig. 1.

Since fractional-order processes naturally exemplify memory consequences, researchers have devised techniques to simulate important considerations using them in recent years [24–33]. Additionally, it has been demonstrated that fractional approaches are effective at analyzing dynamic networks in a variety of disciplines, including banking, neuroscience, and mechanical design [34–36]. Following is a cursory overview of certain significant findings on the pragmatic and hypothetical attributes of differential derivatives. In [37], authors used weak topology to present the formation consequences for Caputo fractional neutral inclusions that avoid compactness in Banach space. The researchers in [38] furnished predictability under prescribed conditions by considering fixed-point hypothesis and fractional calculus methodology. The study [39] presented generalized Mittag-Leffler kernel-based integro-differential equations relying on Atangana–Baleanu fractional derivatives and analyzed the existence-uniqueness of the solutions in Banach space. These research findings have taught us that the defensive actions taken by those who are vulnerable affect how COVID-19 spreads.

Fractional difference equations are effective models for discrete processes with memory effects. Several specific advancements, such as the Riemann and Caputo fractional differences, the fundamentals of discrete fractional calculus, numerical simulations, initial value problems, etc., demonstrated the viewpoint [40]. Implementations of discrete fractional calculus, such as those involving fractional chaotic maps, image encryption, tumor growth and shock frequency, among others, furthermore demonstrate its effectiveness and simplicity [41].

Another approach to determining the fractional sum is on the basis of time scale [42,43]. Both the continuous and discrete-time incidences were generalized. In addition to the Δ -integral on time scales, better characterizations for the mathematical framework were provided [43]. The FDEs are frequently used to illustrate protracted manifestations like fundamental interactions and resource deformability owing to these innovative capabilities [40]. The fractional-order Ψ better describes the transitional state between interfacial tension and pliability. A methodology based on FDE was indicated [41] because sodium chloride exhibits long-term behavior. In addition, there are a few

Table 1
List of parameters.

Symbols	Values	References
π	273 523 621/65 × 365	[49]
\mathbf{v}	0.2	Supposed
\wp_1	1.166×10 ⁻⁸	Supposed
\wp_2	2.101×10 ⁻⁸	Supposed
\wp_3	4.734×10 ⁻⁸	[49]
δ	0.8	Supposed
ς	0.25	Supposed
ρ	0.6	[49]
ϖ	0.4	[50]
v_1	0.33	[50]
v_2	0.1	[50]
η_1	0.01	[51]
η_2	0.033	[52]
ℓ	0.4	Supposed
σ	0.2	Supposed
γ	0.1	Supposed
θ	0.05	Supposed
ρ	1/35 × 365	[53]
ζ	0.11	[54]
β	0.7	[54]
θ_1	0.7	Supposed
θ_2	0.7	Supposed
θ_3	0.7	Supposed
θ_4	0.7	Supposed

other fascinating fields where fractional derivatives are used, including finance, biology, and string theory. Several other fractional formulae have been suggested, including fractional delay DEs, fractional impulsive DEs, fractional interval-valued DEs and fractional difference equations, (see; [42,44–48] and the references cited therein).

However, we are eager to create a fractional difference equations framework to classify the behaviors of COVID-19 taking into account this scenario because the majority of the earlier work has not concentrated on highly vulnerable individuals who follow prevention strategies or do not follow the initiatives. Additionally, we performed an equilibrium evaluation using the model’s simple, persistent restrictions. The ideal method to implement interference strategies was then researched using the framework with time-dependent regulations by assessing their effects and expenditures on the behavior of the COVID-19 disease in actual circumstances in Thailand. It is worth emphasized that each of the aforementioned research findings was formed based on a continuous conduction mode in light of the aforementioned concerns. This phenomenon definitely fascinated us enough to suggest a novel fractional-order discrete model for prevalence and incidence. To the extent we are aware, no research into fractional difference equations for COVID-19 features has been conducted up to this point. In light of the foregoing, the primary goal of this study is to advance the field of epidemiological studies by presenting a novel fractional-order discrete-time COVID-19 framework. Throughout this context, it is important to note that we understand that this framework will, generally, have a range of interesting implementations and standpoints because the suggested framework is merely a discrete fractional version SIR-type scheme and because global epidemic time series can be formed from evolution.

Motivated by the work [55], we initially present our mathematical formula for the COVID-19 disease outbreak utilizing a community split into twelve portions: overall vulnerable (S), heavy vulnerable (S_{10}), moderate vulnerable (S_{20}), heavy susceptible without safety criterion (S_{30}), heavy vulnerable who pursue the precautionary action (S_{40}), and limited vulnerable without a preventing disease (S_{50}), limited vulnerable with immediate concentration on disease prevention (S_{60}), immunized community (\mathcal{V}), exposed population (\mathcal{E}), contagious people to minor side effects (I_1), contagious people who exhibit drastic illnesses (I_{10}) and recovered people \mathcal{R} . This methodology is appropriate for scenarios and public intervention and prevention surveillance programs in Thailand. $\mathcal{N}(\xi) = S(\xi) + S_{10}(\xi) + S_{20}(\xi) + S_{30}(\xi) + S_{40}(\xi) + S_{50}(\xi) +$

$S_{60}(\xi) + \mathcal{V}(\xi) + \mathcal{E}(\xi) + I_1(\xi) + I_{10}(\xi) + \mathcal{R}(\xi)$, with $\xi \in [0, \mathbb{T}]$, represents the entire community at any specific time. Furthermore, we assume that the evolution between these classifications occurs in conformity with the structure shown in Fig. 2.

The attributes of each criterion indicated in the existing scheme, as depicted in Table 1, can be clarified in view of the aforesaid figure.

In fact, the suggested fractional-order discrete COVID-19 model’s infection contamination flow which is depicted in Fig. 2 in its compartmental form can also be characterized by the respective dynamical model:

$$\begin{cases} S(\mathbf{n} + 1) = S(\mathbf{n}) + \pi - (1 + \rho)S(\mathbf{n}), \\ S_{10}(\mathbf{n} + 1) = S_{10}(\mathbf{n}) + \ell S(\mathbf{n}) - (1 + \rho)S_{10}(\mathbf{n}), \\ S_{20}(\mathbf{n} + 1) = S_{20}(\mathbf{n}) + (1 - \ell)S(\mathbf{n}) - (1 + \rho)S_{20}(\mathbf{n}), \\ S_{30}(\mathbf{n} + 1) = S_{30}(\mathbf{n}) + \mathbf{v}S_{10}(\mathbf{n}) - (Y + \theta_1 + \rho)S_{30}(\mathbf{n}), \\ S_{40}(\mathbf{n} + 1) = S_{40}(\mathbf{n}) + (1 - \mathbf{v})S_{10}(\mathbf{n}) - \gamma Y S_{40}(\mathbf{n}) - (\theta_2 + \rho)S_{40}(\mathbf{n}), \\ S_{50}(\mathbf{n} + 1) = S_{50}(\mathbf{n}) + \sigma S_{20}(\mathbf{n}) - \delta Y S_{50}(\mathbf{n}) - (\theta_3 + \rho)S_{50}(\mathbf{n}), \\ S_{60}(\mathbf{n} + 1) = S_{60}(\mathbf{n}) + (1 - \sigma)S_{20}(\mathbf{n}) - \theta Y S_{60}(\mathbf{n}) - (\theta_4 + \rho)S_{60}(\mathbf{n}), \\ \mathcal{V}(\mathbf{n} + 1) = \mathcal{V}(\mathbf{n}) + \theta_1 S_{30}(\mathbf{n}) + \theta_2 S_{40}(\mathbf{n}) + \theta_3 S_{50}(\mathbf{n}) \\ + \theta_4 S_{60}(\mathbf{n}) - (1 - \rho)\varsigma Y \mathcal{V}(\mathbf{n}) - (\rho + \rho)\mathcal{V}(\mathbf{n}), \\ \mathcal{E}(\mathbf{n} + 1) = \mathcal{E}(\mathbf{n}) + Y(S_{30}(\mathbf{n}) + \gamma_2 S_{40}(\mathbf{n}) + \delta S_{50}(\mathbf{n}) + \theta S_{60}(\mathbf{n})) \\ + (1 - \rho)\varsigma Y \mathcal{V}(\mathbf{n}) - (\varpi + \zeta + \rho)\mathcal{E}(\mathbf{n}), \\ I_1(\mathbf{n} + 1) = I_1(\mathbf{n}) + \beta \varpi \mathcal{E}(\mathbf{n}) - (\eta_1 + v_1 + \rho)I_1(\mathbf{n}), \\ I_{10}(\mathbf{n} + 1) = I_{10}(\mathbf{n}) + (1 - \beta)\varpi \mathcal{E}(\mathbf{n}) - (\eta_2 + v_2 + \rho)I_{10}(\mathbf{n}), \\ \mathcal{R}(\mathbf{n} + 1) = \mathcal{R}(\mathbf{n}) + \rho \mathcal{V}(\mathbf{n}) + \zeta \mathcal{E}(\mathbf{n}) + v_1 I_1(\mathbf{n}) + v_2 I_{10}(\mathbf{n}) - \rho \mathcal{R}(\mathbf{n}), \end{cases} \quad (1)$$

supplemented with ICs:

$$\begin{aligned} &S(0), S_{10}(0), S_{20}(0), S_{30}(0), S_{40}(0), S_{50}(0), S_{60}(0), \mathcal{V}(0), \mathcal{E}(0), \\ &I_1(0), I_{10}(0), \mathcal{R}(0) \geq 0. \end{aligned} \quad (2)$$

Here, π signifies the new hiring rate. The following additional factors: ℓ is the percentage of people who are high-risk vulnerable. \mathbf{v} is the percentage of high-risk individuals who do not take precautionary measures seriously. σ is the percentage of limited individuals who do not adhere to the law’s legally required preventative medicine regulations. We have focused on certain experiments that take conventional prevalence, penetration and widespread intervention propagation into account. If we employed the conventional prevalence rate, our vibrant evaluations would have been extremely complicated due to the model’s challenges. Assume that vulnerable people contract the disease at a $Y(\xi)$ rate. The infectious disease strength is classified as $Y(\xi) = \wp_1 \mathcal{E}(\xi) + \wp_2 I_1(\xi) + \wp_3 I_{10}(\xi)$, where \wp_1, \wp_2 and \wp_3 are the propagation levels from \mathcal{E}, I_1 and I_{10} , respectively. The impactful interaction levels of S_{40}, S_{50}, S_{60} and \mathcal{V} are γ, δ, θ and ς , respectively. Their natural fatality rate is indicated by ρ . The value ρ denotes a person’s vaccine effectiveness. The percentage of people who heal normally from \mathcal{E} . ζ is the rate at which people come into contact and are becoming highly contagious. ϖ is the proportion of those who are revealed and \mathcal{V} denotes those who contract an infection. The percentages of healing from infected people with mild signs (I_1) and infected individuals suffering from serious illnesses (I_{10}) are γ_1 and v_2 , respectively. The rate increases of disease-related mortalities in I_1 and I_{10} are η_1 and η_2 , respectively. The vaccination rates for $S_{30}, S_{40}, S_{50}, S_{60}$ are $\theta_1, \theta_2, \theta_3$ and θ_4 , respectively.

The entirety of this article is organized in the following manner: Section “Preliminaries” reviews several fundamental terminologies and key information related to discrete fractional calculus. Section “Qualitative aspects of fractional difference equation model” demonstrates the existence and uniqueness of the finding for the suggested discrete fractional COVID-19 framework using the Picard Lindelöf technique and the fixed point (f_p) hypothesis. In Section “Existence and uniqueness”, we examine the qualitative analysis and stability of the suggested system’s f_p s. Furthermore, the fundamental reproductive number \mathbb{R}_0 for the COVID-19 model is determined. Following Section “Implementation

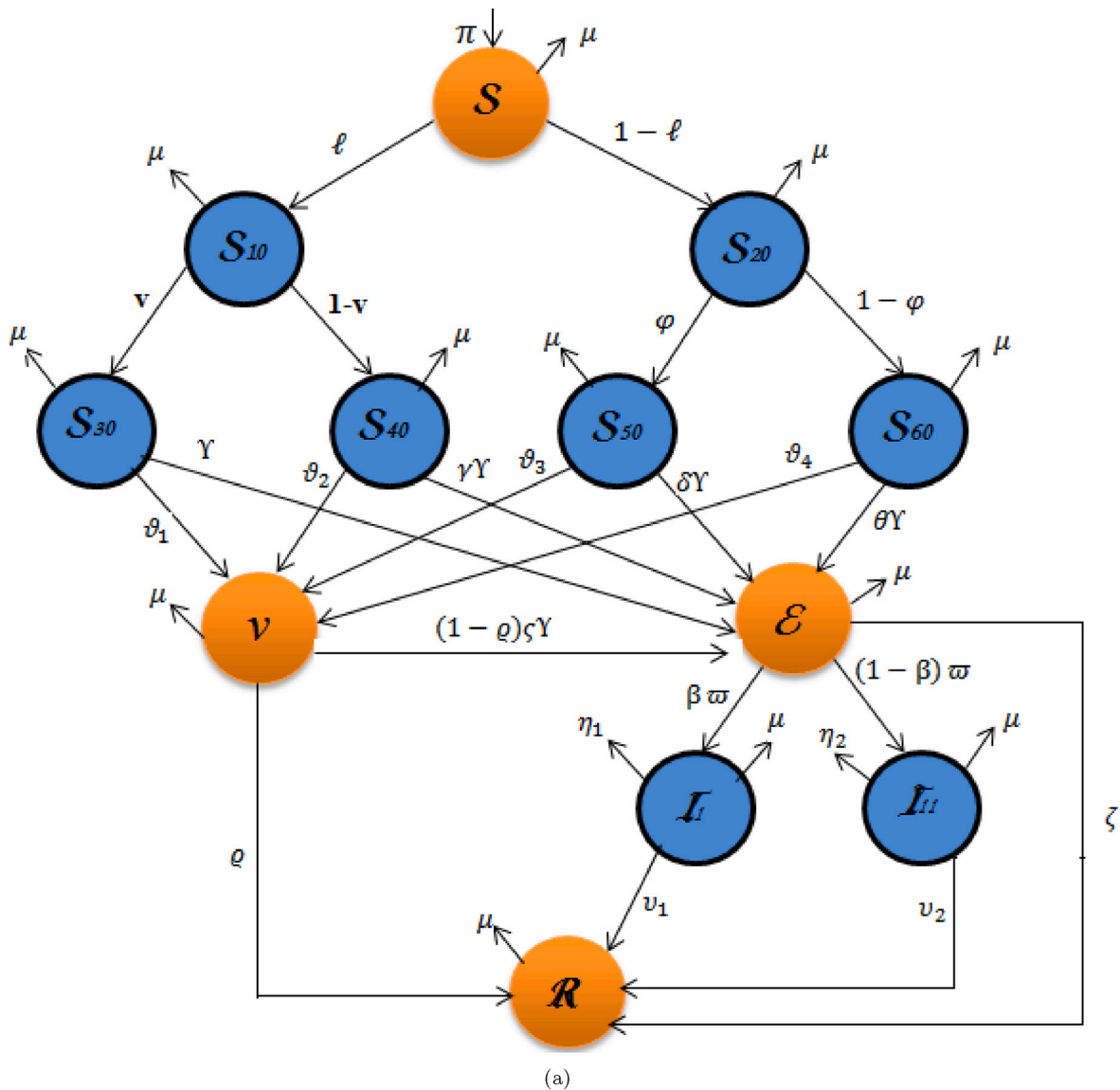


Fig. 2. Schematic view of COVID-19 model.

to estimating COVID-19 behavior”, which summarizes the insights of this task, are certain numerical representations that were run to confirm the mathematical inferences.

Preliminaries

In contrast to classical calculus, fractional calculus has proven to be highly effective in producing quite useful results. This is definitely because of its adaptability and capacity to offer more accurate approximations of a variety of conditions than ever. Moreover, it is helpful to highlight several interpretations and fundamental information related to discrete fractional calculus in providing a more comprehensive view to obtain a deeper comprehension of the fractional-order framework presented in this task and its influence on practise. We will also surmise that the set $\tilde{\mathbb{N}}_c := \{c, c + 1, c + 2, \dots\}$, $c \in \mathbb{R}$ contains definitions for all processes.

Definition 1 ([56]). For $\Psi > 0$, then there is a mapping $g : \tilde{\mathbb{N}}_c \mapsto \mathbb{R}$ with Ψ^{th} -fractional sum is described as

$$\Delta_c^{-\Psi} g(\xi) = \frac{1}{\Gamma(\Psi)} \sum_{\theta=c}^{\xi-\Psi} (\xi - \theta - 1)^{(\Psi-1)} g(\theta), \quad \forall \xi \in \tilde{\mathbb{N}}_{c+\Psi}, \tag{3}$$

where $\Gamma(\cdot)$ is the Euler’s Gamma function and $\xi^{(\Psi)} = \frac{\Gamma(\xi+1)}{\Gamma(\xi+1-\Psi)}$.

Definition 2 ([56]). For $\Psi \in (0, 1)$ and there is Ψ^{th} -order Riemann–Liouville fractional difference formulae of the mapping g is described on $\tilde{\mathbb{N}}_c$ is described as

$$\Delta_c^{\Psi} g(\xi) := \Delta \Delta_c^{-(1-\Psi)} g(\xi) = \frac{1}{\Gamma(1-\Psi)} \Delta \sum_{\theta=c}^{\xi-(1-\Psi)} (\xi - \theta - 1)^{(-\Psi)} g(\theta), \tag{4}$$

$\forall \xi \in \tilde{\mathbb{N}}_{c+1-\Psi}$.

Definition 3 ([56]). For $\Psi \in (0, 1]$ and there is Ψ^{th} -order Caputo fractional difference formulae of the mapping g is described as

$${}^c \Delta_c^{\Psi} g(\xi) := \begin{cases} \Delta \Delta_c^{-(1-\Psi)} g(\xi) = \frac{1}{\Gamma(1-\Psi)} \sum_{\theta=c}^{\xi-(1-\Psi)} (\xi - \theta - 1)^{(-\Psi)} \Delta g(\theta), \\ \forall \xi \in \tilde{\mathbb{N}}_{c+1-\Psi}, \Psi \in (0, 1) \\ \Delta g(\xi), \Psi = 1, \xi \in \tilde{\mathbb{N}}_{c+1-\Psi}. \end{cases} \tag{5}$$

Proposition 1 ([56]). For $\Psi \in (0, 1]$ and suppose that there is a mapping \mathbf{g} defined on $\tilde{\mathbb{N}}_c$. Then

$${}^c \Delta_{c+(1-\Psi)}^\Psi \mathbf{g}(\xi) = \mathbf{g}(\xi) - \mathbf{g}(\mathbf{c}), \quad \forall \xi \in \tilde{\mathbb{N}}_c. \tag{6}$$

Proposition 2 ([56]). For $\Psi \in (0, 1)$ and suppose that there is a mapping \mathbf{g} described on $\tilde{\mathbb{N}}_c$. Then

$${}^c \Delta_c^\Psi \mathbf{g}(\xi) = \Delta_c^\Psi \mathbf{g}(\xi) - \frac{(\xi - \mathbf{c})^{(-\Psi)}}{\Gamma(1-\Psi)} \mathbf{g}(\mathbf{c}), \quad \forall \xi \in \tilde{\mathbb{N}}_{c-\Psi+1}. \tag{7}$$

Lemma 1 ([57]). For $\Psi > 0$, $\Psi \notin \tilde{\mathbb{N}}$ and there is a mapping \mathbf{g} defined on $\tilde{\mathbb{N}}_c$. Then

$$\mathbf{g}(\xi) = \mathbf{g} + \frac{1}{\Gamma(\Psi)} \sum_{r=c+1-\Psi}^{\xi-\Psi} (\xi - r - 1)^{(\Psi-1)} {}^c \Delta_c^\Psi \mathbf{g}(\mathbf{r}), \quad \forall \xi \in \tilde{\mathbb{N}}_{c+1}. \tag{8}$$

Remark 1. The respective states could be seen:

- If ${}^c \Delta_c^\Psi \mathbf{g}(\xi) \geq 0$, then the mapping \mathbf{g} is increasing $\forall \xi \in \tilde{\mathbb{N}}_c$.
- If ${}^c \Delta_c^\Psi \mathbf{g}(\xi) \leq 0$, then the mapping \mathbf{g} is decreasing $\forall \xi \in \tilde{\mathbb{N}}_c$.

Theorem 1 ([58]). Assume that there are two real-valued mappings $\mathbb{k}_1(\xi, \Lambda)$ and $\mathbb{k}_2(\xi, \Lambda)$ described on $[0, \infty) \times \mathbb{R}$. If the mapping \mathbf{k} holds the Lipschitz assumption in Λ having Lipschitz constant \mathcal{L}_ζ such that $\mathcal{L}_\zeta \in (0, \Psi]$, then $\Lambda_1(\xi)$ and $\Lambda_2(\xi)$ are two unique solutions for the subsequent IVP:

$$\begin{cases} \Delta_c^\Psi \Lambda(\xi) = \mathbb{k}_1(\xi + \Psi - 1, \Lambda(\xi + \Psi - 1)), & \xi \in \tilde{\mathbb{N}}_{c+1-\Psi}, \\ \Delta_c^{\Psi-1} \Lambda(\xi) \Big|_{\xi=c} = \Lambda_0, \end{cases} \tag{9}$$

and

$$\begin{cases} \Delta_c^\Psi \Lambda(\xi) = \mathbb{k}_2(\xi + \Psi - 1, \Lambda(\xi + \Psi - 1)), & \xi \in \tilde{\mathbb{N}}_{c+1-\Psi}, \\ \Delta_c^{\Psi-1} \Lambda(\xi) \Big|_{\xi=c} = \Lambda_0. \end{cases} \tag{10}$$

On the basis of the aforementioned hypothesis, the following findings can be made:

- If $\mathbb{k}_1(\xi, \Lambda) < \mathbb{k}_2(\xi, \Lambda)$, then $\Lambda_1(\xi) \leq \Lambda_2(\xi)$ for $\xi \in \tilde{\mathbb{N}}_c$.
- If $\mathbb{k}_1(\xi, \Lambda) > \mathbb{k}_2(\xi, \Lambda)$, then $\Lambda_1(\xi) > \Lambda_2(\xi)$ for $\xi \in \tilde{\mathbb{N}}_c$.

Remark 2. Utilizing the fact of Proposition 1, observing that Theorem 1 is still valid when we transform Δ_c^Ψ by ${}^c \Delta_c^\Psi$.

Furthermore, we can also describe the fractional-order framework in terms of the dynamic system described in (1), which will be considered in this task. The structure of this framework indicates:

$$\begin{cases} {}^c \Delta_0^\Psi S(\xi + 1 - \Psi) = \pi - (1 + \rho)S(\xi), \\ {}^c \Delta_0^\Psi S_{10}(\xi + 1 - \Psi) = \ell S(\xi) - (1 + \rho)S_{10}(\xi), \\ {}^c \Delta_0^\Psi S_{20}(\xi + 1 - \Psi) = (1 - \ell)S(\xi) - (1 + \rho)S_{20}(\xi), \\ {}^c \Delta_0^\Psi S_{30}(\xi + 1 - \Psi) = \mathbf{v}S_{10}(\xi) - (Y + \vartheta_1 + \rho)S_{30}(\xi), \\ {}^c \Delta_0^\Psi S_{40}(\xi + 1 - \Psi) = (1 - \mathbf{v})S_{10}(\xi) - \gamma Y S_{40}(\xi) - (\vartheta_2 + \rho)S_{50}(\xi), \\ {}^c \Delta_0^\Psi S_{50}(\xi + 1 - \Psi) = \sigma S_{20}(\xi) - \delta Y S_{50}(\xi) - (\vartheta_3 + \rho)S_{50}(\xi), \\ {}^c \Delta_0^\Psi S_{60}(\xi + 1 - \Psi) = (1 - \sigma)S_{20}(\xi) - \theta Y S_{60}(\xi) - (\vartheta_4 + \rho)S_{60}(\xi), \\ {}^c \Delta_0^\Psi \mathcal{V}(\xi + 1 - \Psi) = \vartheta_1 S_{30}(\xi) + \vartheta_2 S_{40}(\xi) + \vartheta_3 S_{50}(\xi) + \vartheta_4 S_{60}(\xi) \\ - (1 - \rho)\zeta Y \mathcal{V}(\xi) - (\rho + \rho)\mathcal{V}(\xi), \\ {}^c \Delta_0^\Psi \mathcal{E}(\xi + 1 - \Psi) = Y(S_{30}(\xi) + \gamma_2 S_{40}(\xi) + \delta S_{50}(\xi) + \theta S_{60}(\xi)) \\ + (1 - \rho)\zeta Y \mathcal{V}(\xi) - (\varpi + \zeta + \rho)\mathcal{E}(\xi), \\ {}^c \Delta_0^\Psi I_1(\xi + 1 - \Psi) = \beta \varpi \mathcal{E}(\xi) - (\eta_1 + \nu_1 + \rho)I_1(\xi), \\ {}^c \Delta_0^\Psi I_{10}(\xi + 1 - \Psi) = (1 - \beta)\varpi \mathcal{E}(\xi) - (\eta_2 + \nu_2 + \rho)I_{10}(\xi), \\ {}^c \Delta_0^\Psi \mathcal{R}(\xi + 1 - \Psi) = \rho \mathcal{V}(\xi) + \zeta \mathcal{E}(\xi) + \nu_1 I_1(\xi) + \nu_2 I_{10}(\xi) - \rho \mathcal{R}(\xi), \end{cases} \tag{11}$$

supplemented with ICs:

$$S(0), S_{10}(0), S_{20}(0), S_{30}(0), S_{40}(0), S_{50}(0), S_{60}(0), \mathcal{V}(0), \mathcal{E}(0), I_1(0),$$

$$I_{10}(0), \mathcal{R}(0) \geq 0, \tag{12}$$

where $\Psi \in (0, 1)$ and $\xi \in \tilde{\mathbb{N}}$.

As we continue our investigation, we would like to remind you of a significant finding that confirms the reliability of the model's (11) finding.

Theorem 2 ([59,60]). For $\Psi \in (0, 1)$ and let

$$\mathfrak{S} \in \left\{ \bar{z} \in \mathbb{C} : |\bar{z}| < \left(2 \cos \frac{|\arg \bar{z}| - \pi}{2 - \Psi} \right)^\Psi \text{ and } |\arg \bar{z}| > \frac{\Psi \pi}{2} \right\}, \tag{13}$$

for all eigenvalues \mathfrak{S} of \mathbb{J} , then the \mathbf{f}_p of (11) is asymptotically stable.

Qualitative aspects of fractional difference equation model

In this section, we will discuss the boundedness, positivity, local and global stability and bifurcation analysis of the proposed scheme.

Boundedness

Taking into consideration model (11), for the total populace $\mathcal{N} = S + S_{10} + S_{20} + S_{30} + S_{40} + S_{50} + S_{60} + \mathcal{V} + \mathcal{E} + I_1 + I_{10} + \mathcal{R}$, we can infer the different consequences:

$${}^c \Delta_c^\Psi \mathcal{N}(\xi + 1 - \Psi) = \frac{\pi}{1 + \rho} - \rho \mathcal{N}(\xi) - \eta_1 I_1(\xi) - \eta_2 I_{10}(\xi) \leq \pi - \rho \mathcal{N}(\xi). \tag{14}$$

Consequently, this leads to

$${}^c \Delta_c^\Psi \mathcal{N}(\xi + 1 - \Psi) \leq {}^c \Delta_c^\Psi \mathcal{Y}(\xi + 1 - \Psi), \tag{15}$$

where

$$\begin{cases} {}^c \Delta_c^\Psi \mathcal{Y}(\xi + 1 - \Psi) = \pi - \rho Y_1(\xi), \\ \mathcal{Y}(\mathbf{c}) = \mathcal{N}(\mathbf{c}). \end{cases} \tag{16}$$

As a result, implementing Theorem 1 and Remark 2, it is evident that:

$$\mathcal{N}(\xi) \leq \mathcal{Y}(\xi), \tag{17}$$

that is mainly owing to $\mathcal{N}(\mathbf{c}) \leq \frac{\pi}{\rho(1+\rho)}$. Now, if we consider $\xi^* \in \tilde{\mathbb{N}}_c$ to be the first point where $\mathcal{Y}(\xi^*) > \frac{\pi}{\rho(1+\rho)}$, we get the following:

$$\begin{aligned} \mathcal{Y}(\xi^*) &= \mathcal{Y}(\mathbf{c}) + \frac{1}{\Gamma(\Psi)} \sum_{r=c+1-\Psi}^{\xi^*-\Psi} (\xi^* - r - 1)^{(\Psi-1)} {}^c \Delta_c^\Psi \mathcal{Y}(\mathbf{r}) \\ &= \mathcal{Y}(\mathbf{c}) + \frac{1}{\Gamma(\Psi)} \sum_{r=c+1-\Psi}^{\xi^*-1-\Psi} (\xi^* - r - 1)^{(\Psi-1)} {}^c \Delta_c^\Psi \mathcal{Y}(\mathbf{r}) \\ &\quad + \frac{(\Psi - 1)^{(\Psi-1)}}{\Gamma(\Psi)} {}^c \Delta_c^\Psi \mathcal{Y}(\xi^* - \Psi) \\ &= \mathcal{Y}(\xi^* - 1) + \frac{1}{\Gamma(\Psi)} \sum_{r=c+1-\Psi}^{\xi^*-1-\Psi} \frac{(\xi^* - \mathbf{r} - 1)}{(\xi^* - \mathbf{r} - \Psi)} (\xi^* - \mathbf{r} - 2)^{(\Psi-1)} {}^c \Delta_c^\Psi \mathcal{Y}(\mathbf{r}) \\ &\quad + \frac{(\Psi - 1)^{(\Psi-1)}}{\Gamma(\Psi)} {}^c \Delta_c^\Psi \mathcal{Y}(\xi^* - \Psi) \\ &\leq \mathcal{Y}(\xi^* - 1) + \frac{\pi}{1 + \rho} - \rho \mathcal{Y}(\xi^* - 1) \\ &\leq \frac{\pi}{\rho(1 + \rho)}, \quad \rho + 1 < 1. \end{aligned} \tag{18}$$

Finally, we have a contradiction. As a result of the preceding scenario, we can also demonstrate that if $\rho < 0$, then we have

$$\mathcal{Y}(\xi) \geq 0. \tag{19}$$

This definitely contends that the domain Ω is responsible for the model's (11) solution:

$$\Omega := \left\{ \mathbf{X} \in \mathbb{R}^{12}, 0 \leq \mathbf{x}_i \leq \frac{\pi}{\rho(\rho + 1)}, i = 1, 2, \dots, 12. \right\} \tag{20}$$

It is significant to note that when ρ is small enough, the framework (11) solution is non-negative. The non-negative nature of the scheme (11) solution, moreover, cannot be demonstrated. In fact, the system's solution so often has negative values, but those attributes can later rise to become favorable. Let ξ^* , for instance, be the first point that S is negative, and we get:

$${}^c D_0^\nu S(\xi^* + 1 - \Psi) = \pi - (1 + \rho)S(\xi^*) > 0. \tag{21}$$

As a result, it is evident that the class S will be directly raised in conformity with Remark 1. The remaining compartments can support this claim in an analogous fashion. Despite the fact that such a situation is paradoxical since this system's values should not be negative, it is being discovered that with time, this framework can generate more accurate outcomes. But we shall talk about this supposition subsequently.

Disease-free equilibrium (DFE)

By identifying sufficient requirements associated with the system's (11) specifications to guarantee the stability of this moment, we will also be involved in predicting the reliability of the disease-free fixed point. In order to achieve this, we will start by identifying those DFE points by trying to conflate the right side of framework (11) to zero. Then, we have

$$\tilde{E}_0 = (S^0, S_{10}^0, S_{20}^0, S_{30}^0, S_{40}^0, S_{50}^0, S_{60}^0, \nu^0, 0, 0, 0, \mathcal{R}^0), \tag{22}$$

$$\begin{aligned} \text{where } S^0 &= \frac{\pi}{1+\rho}, S_{10}^0 = \frac{\ell\pi}{(1+\rho)^2}, S_{20}^0 = \frac{(1-\ell)\pi}{(1+\rho)^2}, S_{30}^0 = \frac{\ell\rho\pi}{(\rho+\theta_1)(1+\rho)^2}, S_{40}^0 = \frac{(1-\nu)\ell\pi}{(\rho+\theta_2)(1+\rho)^2}, S_{50}^0 = \frac{\sigma(1-\ell)\pi}{(\theta_3+\rho)(1+\rho)^2}, S_{60}^0 = \frac{(1-\sigma)(1-\ell)\pi}{(\theta_4+\rho)(1+\rho)^2}, \nu^0 = \frac{\theta_1\rho\pi\ell}{(\rho+\theta)(\rho+\theta_1)(1+\rho)^2} + \\ &\frac{\theta_2(1-\nu)\pi\ell}{(\rho+\theta)(\rho+\theta_2)(1+\rho)^2} + \frac{\theta_3\sigma(1-\ell)\pi\ell}{(\rho+\theta)(\rho+\theta_3)(1+\rho)^2} + \frac{\theta_4(1-\sigma)(1-\ell)\pi\ell}{(\rho+\theta)(\rho+\theta_4)(1+\rho)^2}, \text{ and} \\ \mathcal{R}^0 &= \frac{\theta_1\rho\pi\ell}{\rho(\rho+\theta)(\rho+\theta_1)(1+\rho)^2} + \frac{\theta_2(1-\nu)\pi\ell}{\rho(\rho+\theta)(\rho+\theta_2)(1+\rho)^2} + \frac{\theta_3\sigma(1-\ell)\pi\ell}{\rho(\rho+\theta)(\rho+\theta_3)(1+\rho)^2} + \frac{\theta_4(1-\sigma)(1-\ell)\pi\ell}{\rho(\rho+\theta)(\rho+\theta_4)(1+\rho)^2}. \end{aligned}$$

Basic reproduction number

Here, we intend to calculate the basic reproduction number for system (11) using van den Driessche and Watmough's [61] technique. Considering the next-generation matrix as follows:

$$F_{\tilde{E}_0} = \begin{pmatrix} \wp_1\chi & \wp_2\chi & \wp_3\chi \\ 0 & 0 & 0 \\ 0 & 0 & 0 \\ 0 & 0 & 0 \end{pmatrix} \text{ and } \mathcal{V}_{\tilde{E}_0} = \begin{pmatrix} \varpi + \zeta + \rho & 0 & 0 \\ -\Psi\varpi & v_1 + \eta_1 + \rho & 0 \\ -(1-\Psi)\varpi & 0 & v_2 + \eta_2 + \rho \end{pmatrix}, \tag{23}$$

where $\chi = S_{30}^0 + \gamma S_{40}^0 + \delta S_{50}^0 + \theta S_{60}^0 + (1 - \rho)\zeta\nu^0$. The spectral radius of $F\mathcal{V}^{-1}$ is then used to calculate the fundamental reproductive number, which results in

$$\mathbb{R}_0 = \begin{cases} \frac{\rho\ell(\rho+\theta+\theta_1)(1-\rho)\zeta}{(\rho+\theta)(\rho+\theta_1)(1+\rho)^2} + \frac{(1-\nu)\ell\pi(\gamma(\rho+\theta)+\theta_2)(1-\rho)\zeta}{(\rho+\theta)(\rho+\theta_2)(1+\rho)^2} \\ + \frac{\sigma(1-\ell)\pi(\delta(\rho+\theta)+\theta_3)(1-\rho)\zeta}{(\rho+\theta)(\rho+\theta_3)(1+\rho)^2} + \frac{(1-\sigma)(1-\ell)\pi(\theta(\rho+\theta)+\theta_4)(1-\rho)\zeta}{(\rho+\theta)(\rho+\theta_4)(1+\rho)^2} \\ + \frac{(v_2+\eta_2+\rho)(\wp_1(v_1+\eta_1+\rho)+\wp_2\Psi\varpi)+\wp_3\varpi(1-\Psi)(\rho+v_1+\eta_1)}{(\rho+v_1+\eta_1)(\rho+v_2+\eta_2)(\rho+\varpi+\zeta)}. \end{cases} \tag{24}$$

In terms of biology, if $\mathbb{R}_0 < 1$, then the infection will disappear otherwise, if $\mathbb{R}_0 > 1$, the illness will dispersed.

Local and global stability of DFE

In this subsection, we look at the DFE's global asymptotic stability (GAS). In order to achieve this, we highlight the findings presented by Castillo-Chavez et al. [62].

Lemma 2. *Surmise that the framework (11) can be expressed in the form*

$$\begin{aligned} \dot{X}_1(\xi) &= F_1(X_1, X_2), \\ \dot{X}_2(\xi) &= G(X_1, X_2), \quad G(X_1, 0) = 0, \end{aligned} \tag{25}$$

where $X_1 \in \mathbb{R}^n$ signifies the uninfected people and $X_2 \in \mathbb{R}^n$ presents the infected people involving latently infectious. Also, $X_0 = (X_1^*)$ indicates the DFE of the model (11). Furthermore, suppose that the hypothesis (H_1) and (H_2) presented as

- (H_1) For $\dot{X}_1(\xi) = F_1(X_1^*, 0)$, X^* is GAS;
- (H_2) $G(X_1, X_2) = \chi X_2 - \hat{G}(X_1, X_2)$, $\hat{G}(X_1, X_2) \geq 0$ for $(\hat{G}(X_1, X_2)) \in X$, where the Jacobian $\mathcal{A} = \frac{\partial G}{\partial X_2}(X_1^*, 0)$ is an \mathcal{M} -matrix and X_1 is the domain when the framework is biologically plausible.

Thus, the DFE $X_0 = (X^*, 0)$ is GAS.

Now, we put this lemma to use with our framework. It is worth mentioning that from (11), we notice that $\dot{S}_{30} \leq \nu S_{10} - (\rho + \theta_1)S_{30}$, produces $S_{30} \leq \frac{\nu\ell\pi}{(\theta_1+\rho)(1+\rho)^2} = S_{30}^0$, $S_{40} \leq \frac{(1-\nu)\ell\pi}{(\theta_2+\rho)(1+\rho)^2} = S_{40}^0$, $S_{50} \leq \frac{\sigma(1-\ell)\pi}{(\theta_3+\rho)(1+\rho)^2} = S_{50}^0$, $S_{60} \leq \frac{(1-\sigma)(1-\ell)\pi}{(\theta_4+\rho)(1+\rho)^2} = S_{60}^0$, $\nu \leq \frac{\theta_1\nu\ell\pi}{(\rho+\theta)(\rho+\theta_1)(1+\rho)^2} + \frac{\theta_2(1-\nu)\ell\pi}{(\rho+\theta)(\rho+\theta_2)(1+\rho)^2} + \frac{\theta_3\sigma(1-\ell)\pi}{(\rho+\theta)(\rho+\theta_3)(1+\rho)^2} + \frac{\theta_4(1-\sigma)(1-\ell)\pi}{(\rho+\theta)(\rho+\theta_4)(1+\rho)^2} = \nu^0$.

Theorem 3. *The DFE of the model (11) is GAS if $\mathbb{R}_0 < 1$.*

Proof. Justifying Lemma 3 and confirming the assumptions (H_1) and (H_2) . In accordance with the ordinary DEs, we have $X_1 = (S, S_{10}, S_{20}, S_{30}, S_{40}, S_{50}, S_{60}, \nu^0)^T$ and $X_2 = (S^0, S_{10}^0, S_{20}^0, S_{30}^0, S_{40}^0, S_{50}^0, S_{60}^0, \nu^0)^T$. Since $Y(\xi) = \wp_1\mathcal{E}(\xi) + \wp_2I_{10}(\xi) + \wp_3I_{10}(\xi)$, so that at the DFE point $Y = 0$. Observe that

$$\dot{X}_1 = F_1(X_1, 0) = \begin{pmatrix} \pi - (1 + \rho)S \\ \ell S - (1 + \rho)S_{10} \\ (1 - \ell)S - (1 + \rho)S_{20} \\ \nu S_{10} - (\theta_1 + \rho)S_{30} \\ (1 - \nu)S_{10} - (\theta_2 + \rho)S_{40} \\ \sigma S_{20} - (\theta_3 + \rho)S_{50} \\ (1 - \sigma)S_{20} - (\theta_4 + \rho)S_{60} \\ \theta_1 S_{30} + \theta_2 S_{40} + \theta_3 S_{50} + \theta_4 S_{60} - (\rho + \theta)\nu \end{pmatrix} \tag{26}$$

is linear and its response is simple to find as follows:

$$\begin{aligned} S(\xi) &= S^0 + c_0 \exp(- (1 + \rho)\xi), \quad S_{10}(\xi) = S_{10}^0 + (c_0\ell\xi + c_1) \exp(- (1 + \rho)\xi), \\ S_{20}(\xi) &= S_{20}^0 + ((1 - \ell)c_0\xi + c_2) \exp(- (1 + \rho)\xi), \\ S_{30}(\xi) &= S_{30}^0 + \left\{ \int (c_0\ell\theta + c_1)\nu \exp(- (1 - \theta_1)\theta)d\theta \right\} \exp(- (\theta_1 + \rho)\xi), \\ S_{40}(\xi) &= S_{40}^0 + \left\{ \int (c_0\ell\theta + c_1)(1 - \nu) \exp(- (1 - \theta_2)\theta)d\theta \right\} \\ &\exp(- (\theta_2 + \rho)\xi), \\ S_{50}(\xi) &= S_{50}^0 + \left\{ \int ((1 - \ell)c_0\theta + c_2)\sigma \exp(- (1 - \theta_3)\theta)d\theta \right\} \\ &\exp(- (\theta_3 + \rho)\xi), \\ S_{60}(\xi) &= S_{60}^0 + \left\{ \int ((1 - \ell)c_0\theta + c_2)(1 - \sigma) \right. \\ &\left. \exp(- (1 - \theta_4)\theta)d\theta \right\} \exp(- (\theta_4 + \rho)\xi), \\ \nu(\xi) &= \nu^0 + \left\{ \int \int (c_0\ell\theta + c_1)\theta_1\nu \exp(- (1 - \theta_1)\theta)d\theta \right. \\ &\left. \exp(- (\theta_1 - \rho)r)dr \right\} \exp(- (\rho + \theta)\xi) \\ &+ \left\{ \int \int (c_0\ell\theta + c_1)\theta_2(1 - \nu) \exp(- (1 - \theta_2)\theta)d\theta \exp(- (\theta_2 - \rho)r)dr \right\} \\ &\exp(- (\rho + \theta)\xi) \\ &+ \left\{ \int \int (c_0(1 - \ell)\theta + c_2)\theta_3\sigma \exp(- (1 - \theta_3)\theta)d\theta \exp(- (\theta_3 - \rho)r)dr \right\} \\ &\exp(- (\rho + \theta)\xi) \\ &+ \left\{ \int \int (c_0(1 - \ell)\theta + c_1)\theta_4(1 - \sigma) \exp(- (1 - \theta_4)\theta)d\theta \right. \\ &\left. \exp(- (\theta_4 - \rho)r)dr \right\} \exp(- (\rho + \theta)\xi). \end{aligned} \tag{27}$$

Evidently, $(S(\xi), S_{10}(\xi), S_{20}(\xi), S_{30}(\xi), S_{40}(\xi), S_{50}(\xi), S_{60}(\xi), \mathcal{V}(\xi)) \mapsto (S^0, S_{10}^0, S_{20}^0, S_{30}^0, S_{40}^0, S_{50}^0, S_{60}^0, \mathcal{V}^0)$, as $\xi \mapsto \infty$ and c_0, c_1, c_2 are fixed constants. Therefore, $\mathbf{X}_1^* = (S^0, S_{10}^0, S_{20}^0, S_{30}^0, S_{40}^0, S_{50}^0, S_{60}^0, \mathcal{V}^0)$ is GAS for (11).

Furthermore, we have

$$\mathcal{G}(\mathbf{X}_1, \mathbf{X}_2) = \begin{pmatrix} (S_{30} + \gamma S_{40} + \delta S_{50} + \theta S_{60} + (1 - \rho)\zeta\mathcal{V})Y - (\varpi + \zeta + \rho)\mathcal{E} \\ \beta\varpi\mathcal{E} - (v_1 + \eta_1 + \rho)I_1 \\ (1 - \beta)\varpi\mathcal{E} - (v_2 + \eta_2 + \rho)I_{10} \end{pmatrix}. \tag{28}$$

Suppose that $\bar{A} = S_{30}^0 + \gamma S_{40}^0 + \delta S_{50}^0 + \theta S_{60}^0 + (1 - \rho)\zeta\mathcal{V}^0$.

Consequently, we can get

$$\bar{A} = \begin{pmatrix} \wp_1\bar{A} - (\varpi + \zeta + \rho) & \wp_2\bar{A} & \wp_3\bar{A} \\ \beta\varpi & -(v_1 + \eta_1 + \rho) & 0 \\ (1 - \beta)\varpi & 0 & -(v_2 + \eta_2 + \rho) \end{pmatrix} \tag{29}$$

that is straightforwardly an \mathcal{M} -matrix. In the meantime, we know that

$$\mathcal{G}(\mathbf{X}_1, \mathbf{X}_2) = \begin{pmatrix} ((S_{30}^0 - S_{30}) + \gamma(S_{40}^0 - S_{40}) + \delta(S_{50}^0 - S_{50}) + \theta(S_{60}^0 - S_{60}) + (1 - \rho)\zeta(\mathcal{V}^0 - \mathcal{V}))Y \\ 0 \\ 0 \end{pmatrix}. \tag{30}$$

This is indeed the case $S_{30}^0 \geq S_{30} \geq 0, S_{40}^0 \geq S_{40} \geq 0, S_{50}^0 \geq S_{50} \geq 0, S_{60}^0 \geq S_{60} \geq 0, \mathcal{V}^0 \geq \mathcal{V} \geq 0$. Therefore, the DFE $\mathbf{X}_0 = (\mathbf{X}_*, 0)$ is GAS. \square

Endemic equilibrium (EE)

While the stability at the EE is for the long-term complexities when the illness lingers and $\mathbb{R}_0 > 1$, the stability at the DFE is for the short-term outbreaks of the ailment. We will examine the systemic characteristics of our framework in this portion.

We start by investigating to determine whether the non-negative EE exists. Suppose that

$$\begin{aligned} F_1(\mathcal{E}^*) &= \wp_1\mathcal{E}^* + \frac{\wp_2\beta\varpi\mathcal{E}^*}{v_1 + \eta_1 + \rho} + \frac{\wp_3(1 - \beta)\varpi\mathcal{E}^*}{v_2 + \eta_2 + \rho}, \\ f_{F_2}(\mathcal{E}^*) &= (F_1(\mathcal{E}^*) + \rho + \vartheta_1)(1 + \rho)^2, \\ F_3(\mathcal{E}^*) &= (\gamma F_1(\mathcal{E}^*) + \rho + \vartheta_2)(1 + \rho)^2, \quad F_4(\mathcal{E}^*) = (\delta F_1(\mathcal{E}^*) + \rho + \vartheta_3)(1 + \rho)^2, \\ F_5(\mathcal{E}^*) &= (\theta F_1(\mathcal{E}^*) + \rho + \vartheta_4)(1 + \rho)^2, \quad F_6(\mathcal{E}^*) = (\zeta(1 - \rho)F_1(\mathcal{E}^*) + \rho + \varrho). \end{aligned} \tag{31}$$

The system's (11) EE is represented by $\bar{E}^* = (S^*, S_{10}^*, S_{20}^*, S_{30}^*, S_{40}^*, S_{50}^*, S_{60}^*, \mathcal{V}^*, I_1^*, I_{10}^*, \mathcal{R}^*)^T$, where

$$\begin{aligned} S^* &= \frac{\pi}{1 + \rho}, \quad S_{10}^* = \frac{\ell\pi}{(1 + \rho)^2}, \quad S_{20}^* = \frac{(1 - \ell)\pi}{(1 + \rho)^2}, \quad S_{30}^* = \frac{\mathbf{v}\ell\pi}{F_2(\mathcal{E}^*)}, \\ S_{40}^* &= \frac{(1 - \mathbf{v})\ell\pi}{F_3(\mathcal{E}^*)}, \\ S_{50}^* &= \frac{\sigma(1 - \ell)\pi}{F_4(\mathcal{E}^*)}, \quad S_{60}^* = \frac{(1 - \sigma)(1 - \ell)\pi}{F_5(\mathcal{E}^*)}, \\ \mathcal{E}^* &= \frac{(S_{30}^* + \gamma S_{40}^* + \delta S_{50}^* + \theta S_{60}^* + (1 - \rho)\zeta\mathcal{V}^*)}{\varpi + \zeta + \rho}, \\ \mathcal{V}^* &= \frac{1}{F_6(\mathcal{E}^*)} \left\{ \vartheta_1 \frac{\mathbf{v}\ell\pi}{F_2(\mathcal{E}^*)} + \vartheta_2 \frac{(1 - \mathbf{v})\ell\pi}{F_3(\mathcal{E}^*)} + \vartheta_3 \frac{\sigma(1 - \ell)\pi}{F_4(\mathcal{E}^*)} \right. \\ &\quad \left. + \vartheta_4 \frac{(1 - \sigma)(1 - \ell)\pi}{F_5(\mathcal{E}^*)} \right\}, \\ I_1^* &= \frac{\beta\varpi\mathcal{E}^*}{\rho + \eta_1 + v_1}, \quad I_{10}^* = \frac{(1 - \beta)\varpi\mathcal{E}^*}{\rho + \eta_2 + v_2}. \end{aligned} \tag{32}$$

Also, we suppose that $f_1(\mathcal{E})$,

$$f_1(\mathcal{E}) =$$

$$\left\{ \frac{\wp_1(\rho + \eta_1 + v_1)(\rho + \eta_2 + v_2) + \wp_2\beta\varpi(\rho + \eta_2 + v_2) + \wp_3(1 - \beta)\varpi(\rho + \eta_1 + v_1)}{(\rho + \eta_1 + v_1)(\rho + \eta_2 + v_2)} \right\} \mathcal{E}. \tag{33}$$

When we transform (33) into \mathcal{E}^* for $\mathcal{E} = \mathcal{E}^*$, we have $h_1(\mathcal{E}) = h_2(\mathcal{E})$, where

$$\begin{aligned} h_1(\mathcal{E}) &= \frac{(\rho + \eta_1 + v_1)(\rho + \eta_2 + v_2)(\varpi + \zeta + \rho)}{\wp_1(\rho + \eta_1 + v_1)(\rho + \eta_2 + v_2) + \wp_2\beta\varpi(\rho + \eta_2 + v_2) + \wp_3(1 - \beta)\varpi(\rho + \eta_1 + v_1)}, \\ h_2(\mathcal{E}) &= \frac{\mathbf{v}\ell\pi}{F_2(\mathcal{E}^*)} + \frac{\gamma(1 - \mathbf{v})\ell\pi}{F_3(\mathcal{E}^*)} + \frac{\delta\sigma(1 - \ell)\pi}{F_4(\mathcal{E}^*)} + \frac{\theta(1 - \sigma)(1 - \ell)\pi}{F_5(\mathcal{E}^*)} \\ &\quad + \frac{(1 - \rho)\zeta}{F_6(\mathcal{E}^*)} \left\{ \vartheta_1 \frac{\mathbf{v}\ell\pi}{F_2(\mathcal{E}^*)} + \vartheta_2 \frac{(1 - \mathbf{v})\ell\pi}{F_3(\mathcal{E}^*)} + \vartheta_3 \frac{\sigma(1 - \ell)\pi}{F_4(\mathcal{E}^*)} \right. \\ &\quad \left. + \vartheta_4 \frac{(1 - \sigma)(1 - \ell)\pi}{F_5(\mathcal{E}^*)} \right\}. \end{aligned} \tag{34}$$

Obviously, both h_1 and h_2 are differentiable mappings for $\mathcal{E} \geq 0$. Clearly, $F_2(\mathcal{E}) > 0, F_3(\mathcal{E}) > 0, F_4(\mathcal{E}) > 0, F_5(\mathcal{E}) > 0$ also, $F_2'(\mathcal{E}) > 0, F_3'(\mathcal{E}) > 0, F_4'(\mathcal{E}) > 0, F_5'(\mathcal{E}) > 0$. Following is the outcome of computing the derivative of h_1 and h_2 :

$$\begin{aligned} h_1'(\mathcal{E}) &= 0, \\ h_2'(\mathcal{E}) &= \frac{\mathbf{v}\ell\pi F_2'(\mathcal{E})}{(F_2(\mathcal{E}))^2} - \frac{\gamma(1 - \mathbf{v})\ell\pi F_3'(\mathcal{E})}{(F_3(\mathcal{E}))^2} - \frac{\delta\sigma(1 - \ell)\pi F_4'(\mathcal{E})}{(F_4(\mathcal{E}))^2} \\ &\quad - \frac{\theta(1 - \sigma)(1 - \ell)\pi F_5'(\mathcal{E})}{(F_5(\mathcal{E}))^2} \\ &\quad + \frac{(1 - \rho)\zeta}{F_6(\mathcal{E}^*)} \left\{ \frac{\vartheta_1 \mathbf{v}\ell\pi F_2'(\mathcal{E})}{(F_2(\mathcal{E}))^2} + \frac{\vartheta_2(1 - \mathbf{v})\ell\pi F_3'(\mathcal{E})}{(F_3(\mathcal{E}))^2} \right. \\ &\quad \left. + \frac{\vartheta_3\sigma(1 - \ell)\pi F_4'(\mathcal{E})}{(F_4(\mathcal{E}))^2} + \frac{\vartheta_4(1 - \sigma)(1 - \ell)\pi F_5'(\mathcal{E})}{(F_5(\mathcal{E}))^2} \right\} \\ &\quad - \frac{(1 - \rho)\zeta F_6'(\mathcal{E})}{F_6(\mathcal{E}^*)} \left\{ \frac{\vartheta_1 \mathbf{v}\ell\pi}{F_2(\mathcal{E}^*)} + \frac{\vartheta_2(1 - \mathbf{v})\ell\pi}{F_3(\mathcal{E}^*)} + \frac{\vartheta_3\sigma(1 - \ell)\pi}{F_4(\mathcal{E}^*)} \right. \\ &\quad \left. + \frac{\vartheta_4(1 - \sigma)(1 - \ell)\pi}{F_5(\mathcal{E}^*)} \right\} < 0. \end{aligned} \tag{35}$$

Therefore, $h_1(\mathcal{E})$ is an increasing straight line on $[0, \infty]$, and $h_2(\mathcal{E})$ is a nonincreasing one. To evaluate whether the two curves interconnect and, consequently, whether a non-negative EE persists, we can make comparisons of their vertical intercepts. We can conveniently see that there is a particular EE of $\bar{E} = \bar{E}^*$ if $\mathbb{R}_0 > 1$, then $h_1(0) < h_2(0)$. There is no EE, though, if $\mathbb{R}_0 \leq 1$ because $h_1(0) > h_2(0)$.

Global stability of EE

Next, we will analyze the GAS of the EE using the geometric methodology first put forth by Lyapunov and La Salle–Lyapunov [63]. In order to achieve this, we begin by presenting the following outcome in accordance with the geometric technique:

Theorem 4. *The unique EE \bar{E}^* of (11) is GAS whenever $\mathbb{R}_0 > 1$.*

Proof. We will demonstrate that \bar{E}^* is globally stable. We begin by contemplating about the respective expression:

$$\mathfrak{L}(A) = A - A^* + A^* \ln\left(\frac{A}{A^*}\right) \tag{36}$$

for $A, A^* > 0$. Replacing A by the all cohorts of the model (11). Evidently, $\mathfrak{L}(A) \geq 0$ form the identity if and only if $A = A^*$. Suppose $Y = \wp_1\mathcal{E} + \wp_2I_1 + \wp_3I_{10}$.

Performing differentiation of the function $\mathfrak{L}(A)$ after inserting all compartments of the model (11) and employing the equilibrium conditions produces

$$\begin{aligned} \dot{\mathfrak{L}}(S)(\xi) &= (1 + \rho) \left(\frac{S - S^*}{S} \right) (S^* - S) + \ell \left(\frac{S_{10} - S_{10}^*}{S_{10}} \right) \left(\frac{SS_{10}^* - S^*S_{10}}{S_{10}^*} \right) \\ &\quad + (1 - \ell) \left(\frac{S_{20} - S_{20}^*}{S_{20}} \right) \left(\frac{SS_{20}^* - S^*S_{20}}{S^*} \right) \end{aligned}$$

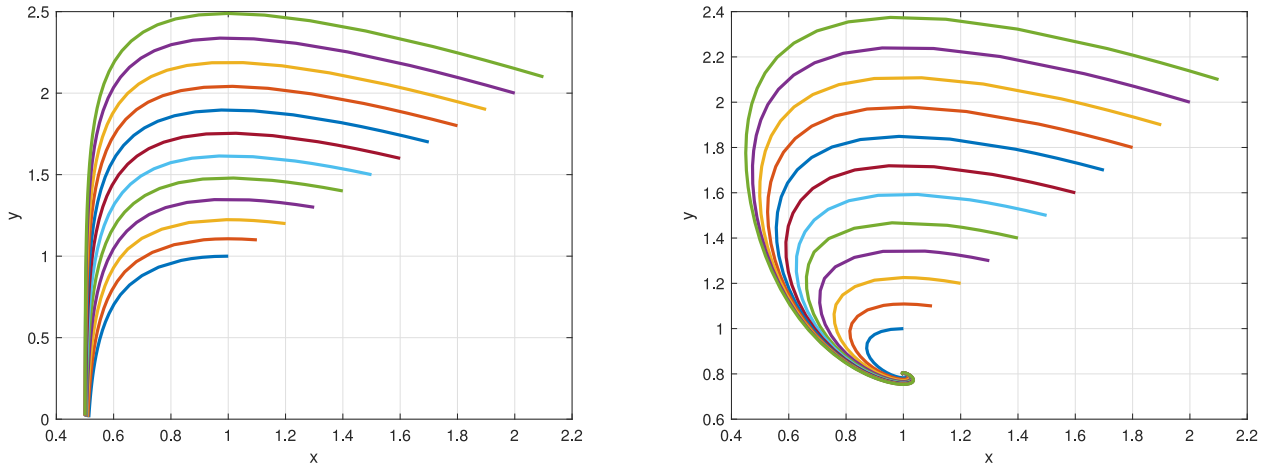


Fig. 3. Graphical view for all initial exposed peoples. It is evident that every graph leads to an EE point. This modeling was functioning. We furthermore ran a test run for a longer time frame, and the outcome was equivalent. Graphical view of (a) S vs. \mathcal{E} (b) A phase comparison of \mathcal{E} and I .

$$\begin{aligned} &\leq (1 + \rho)S^* \left(\frac{2SS^* - S^{*2} - S^2}{SS^*} \right) \\ &+ \ell S^* \left(\frac{2SS_{10}S^*S_{10}^* - S_{10}^{*2}S^2 - S_{10}^2S^{*2}}{SS_{10}S^*S_{10}^*} \right) \\ &+ (1 - \ell)S^* \left(\frac{2SS_{20}S^*S_{20}^* - S_{20}^{*2}S^2 - S_{20}^2S^{*2}}{SS_{20}S^*S_{20}^*} \right). \end{aligned} \tag{37}$$

The final variant results from the suppositions that

$$S_{10}S^* \leq SS_{10}^* \text{ and } S^* \geq S.$$

Therefore, getting it is simple

$$(S_{10}S^* - SS_{10}^*)(S^* - S) \leq 0, \text{ as } S > 0. \tag{38}$$

Assume that

$$\begin{aligned} \frac{d\mathcal{L}(S_{30})}{d\xi} &= \left(\frac{S_{30}^* - S_{30}}{S_{30}} \right) \left\{ \nu S_{10} - \gamma S_{30} - \nu S_{10}^* \frac{S_{30}^*}{S_{30}} + \gamma^* S_{30} \right\} \\ &\leq \nu S_{10}^* \left(\frac{S_{10}}{S_{10}^*} - \frac{S_{10}S_{30}^*}{S_{10}^*S_{30}} - \frac{S_{30}}{S_{30}^*} + 1 \right) \\ &+ \gamma^* S_{30}^* \left(\frac{S_{30}}{S_{30}^*} - \frac{\gamma S_{30}}{\gamma^* S_{30}^*} + \frac{\gamma}{\gamma^*} - 1 \right). \end{aligned} \tag{39}$$

Analogously, we have

$$\begin{aligned} \frac{d\mathcal{L}(S_{40})}{d\xi} &\leq (1 - \nu)S_{10}^* \left(\frac{S_{10}}{S_{10}^*} - \frac{S_{10}S_{40}^*}{S_{10}^*S_{40}} - \frac{S_{40}}{S_{40}^*} + 1 \right) \\ &+ \gamma\gamma^* S_{40}^* \left(\frac{S_{40}}{S_{40}^*} - \frac{\gamma S_{40}}{\gamma^* S_{40}^*} + \frac{\gamma}{\gamma^*} - 1 \right), \\ \frac{d\mathcal{L}(S_{50})}{d\xi} &\leq \sigma S_{20}^* \left(\frac{S_{20}}{S_{20}^*} - \frac{S_{20}S_{40}^*}{S_{20}^*S_{40}} - \frac{S_{50}}{S_{50}^*} + 1 \right) \\ &+ \delta\gamma^* S_{50}^* \left(\frac{S_{50}}{S_{50}^*} - \frac{\gamma S_{50}}{\gamma^* S_{50}^*} + \frac{\gamma}{\gamma^*} - 1 \right), \\ \frac{d\mathcal{L}(S_{60})}{d\xi} &\leq (1 - \sigma)S_{20}^* \left(\frac{S_{20}}{S_{20}^*} - \frac{S_{20}S_{60}^*}{S_{20}^*S_{60}} - \frac{S_{60}}{S_{60}^*} + 1 \right) \\ &+ \theta\gamma^* S_{60}^* \left(\frac{S_{60}}{S_{60}^*} - \frac{\gamma S_{60}}{\gamma^* S_{60}^*} + \frac{\gamma}{\gamma^*} - 1 \right), \\ \frac{d\mathcal{L}(\mathcal{V})}{d\xi} &\leq \vartheta_1 S_{30}^* \left(\frac{S_{30}}{S_{30}^*} - \frac{S_{30}\mathcal{V}^*}{S_{30}^*\mathcal{V}} - \frac{\mathcal{V}}{\mathcal{V}^*} + 1 \right) \\ &+ \vartheta_2 S_{40}^* \left(\frac{S_{40}}{S_{40}^*} - \frac{S_{40}\mathcal{V}^*}{S_{40}^*\mathcal{V}} - \frac{\mathcal{V}}{\mathcal{V}^*} + 1 \right) \end{aligned}$$

$$\begin{aligned} &+ \vartheta_3 S_{50}^* \left(\frac{S_{50}}{S_{50}^*} - \frac{S_{50}\mathcal{V}^*}{S_{50}^*\mathcal{V}} - \frac{\mathcal{V}}{\mathcal{V}^*} + 1 \right) \\ &+ \vartheta_4 S_{60}^* \left(\frac{S_{60}}{S_{60}^*} - \frac{S_{60}\mathcal{V}^*}{S_{60}^*\mathcal{V}} - \frac{\mathcal{V}}{\mathcal{V}^*} + 1 \right) \\ &+ (1 - \rho)\zeta\gamma^*\mathcal{V}^* \left(\frac{\mathcal{V}}{\mathcal{V}^*} - \frac{\gamma\mathcal{V}}{\gamma^*\mathcal{V}^*} - \frac{\gamma}{\gamma^*} - 1 \right), \\ \frac{d\mathcal{L}(\mathcal{E})}{d\xi} &\leq \gamma^* S_{30}^* \left(\frac{\gamma S_{30}}{\gamma^* S_{30}^*} - \frac{\gamma S_{30}\mathcal{E}^*}{\gamma^* S_{30}^* \mathcal{E}^*} - \frac{\mathcal{E}}{\mathcal{E}^*} + 1 \right) \\ &+ \gamma\gamma^* S_{40}^* \left(\frac{\gamma S_{40}}{\gamma^* S_{40}^*} - \frac{\gamma S_{40}\mathcal{E}^*}{\gamma^* S_{40}^* \mathcal{E}^*} - \frac{\mathcal{E}}{\mathcal{E}^*} + 1 \right) \\ &+ \delta\gamma^* S_{50}^* \left(\frac{\gamma S_{50}}{\gamma^* S_{50}^*} - \frac{\gamma S_{50}\mathcal{E}^*}{\gamma^* S_{50}^* \mathcal{E}^*} - \frac{\mathcal{E}}{\mathcal{E}^*} + 1 \right) \\ &+ \zeta\gamma^* S_{60}^* \left(\frac{\gamma S_{60}}{\gamma^* S_{60}^*} - \frac{\gamma S_{60}\mathcal{E}^*}{\gamma^* S_{60}^* \mathcal{E}^*} - \frac{\mathcal{E}}{\mathcal{E}^*} + 1 \right) \\ &+ (1 - \rho)\zeta\gamma^*\mathcal{V}^* \left(\frac{\gamma\mathcal{V}}{\gamma^*\mathcal{V}^*} - \frac{\gamma\mathcal{V}\mathcal{E}^*}{\gamma^*\mathcal{V}^* \mathcal{E}^*} - \frac{\mathcal{E}}{\mathcal{E}^*} + 1 \right), \\ \frac{d\mathcal{L}(I_1)}{d\xi} &\leq \beta\varpi\mathcal{E}^* \left(\frac{2\mathcal{E}\mathcal{E}^*I_1I_1^* - \mathcal{E}^2(I_1^*)^2 - (\mathcal{E}^*)^2(I_1)^2}{\mathcal{E}\mathcal{E}^*I_1I_1^*} \right), \\ \frac{d\mathcal{L}(I_{10})}{d\xi} &\leq (1 - \beta)\varpi\mathcal{E}^* \left(\frac{2\mathcal{E}\mathcal{E}^*I_{10}I_{10}^* - \mathcal{E}^2(I_{10}^*)^2 - (\mathcal{E}^*)^2(I_{10})^2}{\mathcal{E}\mathcal{E}^*I_{10}I_{10}^*} \right). \end{aligned} \tag{40}$$

In view of the Lyapunov candidate, we have

$$\begin{aligned} \mathcal{L}(\xi) &= \mathcal{L}(S) + \mathcal{L}(S_{10}) + \mathcal{L}(S_{20}) + \mathcal{L}(S_{30}) + \mathcal{L}(S_{40}) + \mathcal{L}(S_{50}) \\ &+ \mathcal{L}(S_{60}) + \mathcal{L}(\mathcal{V}) + \mathcal{L}(\mathcal{E}) \\ &+ \mathcal{L}(I_1) + \mathcal{L}(I_{10}). \end{aligned} \tag{41}$$

The system's (11) solutions are determined by \mathcal{L} 's derivative, which results in

$$\begin{aligned} \frac{d\mathcal{L}}{d\xi} &\leq (1 + \rho)S^* \left(\frac{2SS^* - S^{*2} - S^2}{SS^*} \right) \\ &+ \ell S^* \left(\frac{2SS_{10}S^*S_{10}^* - S_{10}^{*2}S^2 - S_{10}^2S^{*2}}{SS_{10}S^*S_{10}^*} \right) \\ &+ (1 - \ell)S^* \left(\frac{2SS_{20}S^*S_{20}^* - S_{20}^{*2}S^2 - S_{20}^2S^{*2}}{SS_{20}S^*S_{20}^*} \right) \\ &+ \nu S_{10}^* \left(\frac{S_{10}}{S_{10}^*} - \frac{S_{10}S_{30}^*}{S_{10}^*S_{30}} - \frac{S_{30}}{S_{30}^*} + 1 \right) \end{aligned}$$

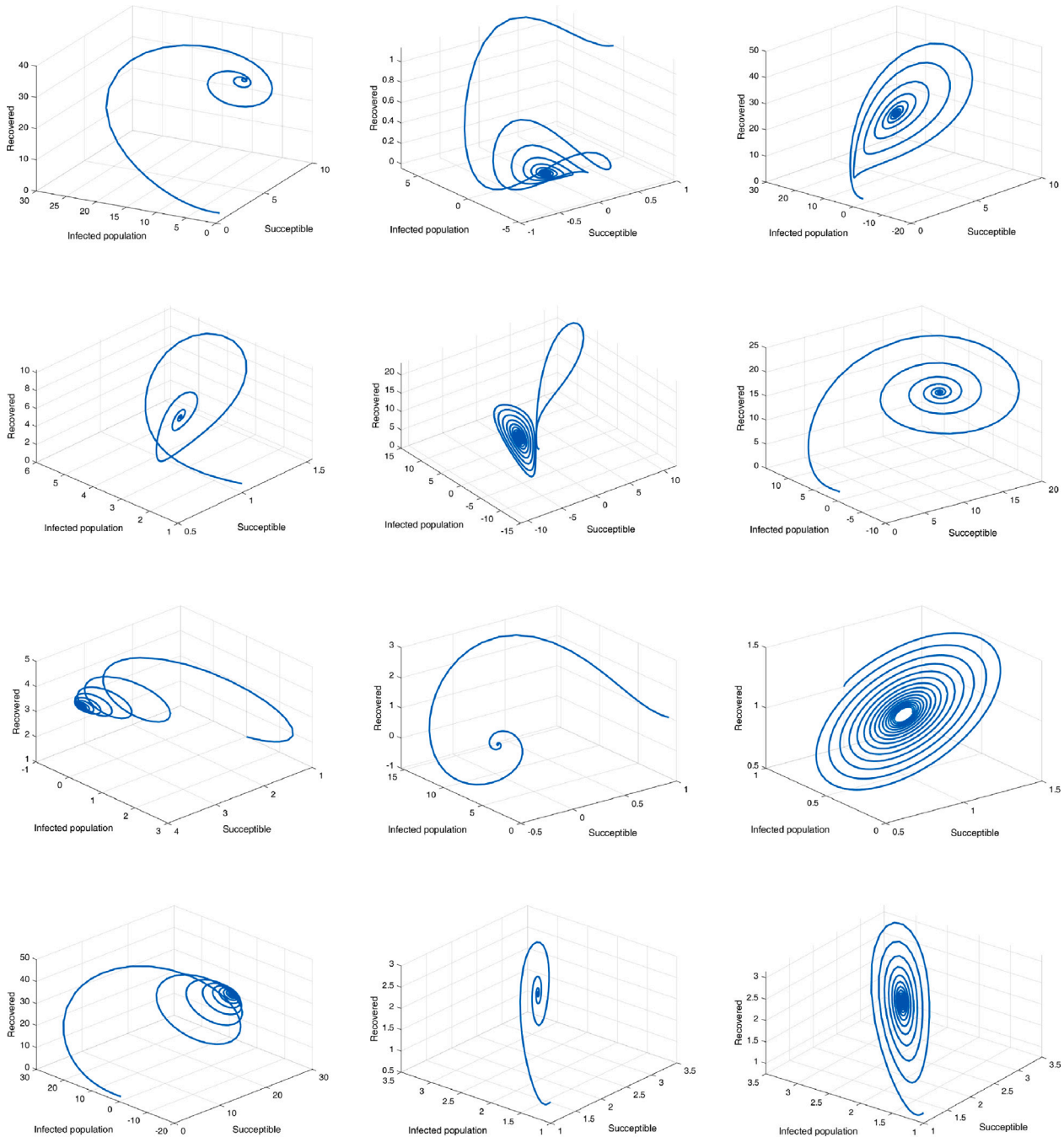


Fig. 4. Phase portraits of EE \bar{E}_1 for various fractional-order derivatives having stability $\mathbb{R}_0 > 1$.

$$\begin{aligned}
 &+Y^*S_{30}^* \left(\frac{S_{30}}{S_{30}^*} - \frac{YS_{30}}{Y^*S_{30}^*} + \frac{Y}{Y^*} - 1 \right) \\
 &+(1-\nu)S_{10}^* \left(\frac{S_{10}}{S_{10}^*} - \frac{S_{10}S_{40}^*}{S_{10}^*S_{40}} - \frac{S_{40}}{S_{40}^*} + 1 \right) \\
 &+\gamma Y^*S_{40}^* \left(\frac{S_{40}}{S_{40}^*} - \frac{YS_{40}}{Y^*S_{40}^*} + \frac{Y}{Y^*} - 1 \right) \\
 &+\sigma S_{20}^* \left(\frac{S_{20}}{S_{20}^*} - \frac{S_{20}S_{40}^*}{S_{20}^*S_{40}} - \frac{S_{50}}{S_{50}^*} + 1 \right)
 \end{aligned}$$

$$\begin{aligned}
 &+\delta Y^*S_{50}^* \left(\frac{S_{50}}{S_{50}^*} - \frac{YS_{50}}{Y^*S_{50}^*} + \frac{Y}{Y^*} - 1 \right) \\
 &+(1-\sigma)S_{20}^* \left(\frac{S_{20}}{S_{20}^*} - \frac{S_{20}S_{60}^*}{S_{20}^*S_{60}} - \frac{S_{60}}{S_{60}^*} + 1 \right) \\
 &+\theta Y^*S_{60}^* \left(\frac{S_{60}}{S_{60}^*} - \frac{YS_{60}}{Y^*S_{60}^*} + \frac{Y}{Y^*} - 1 \right) \\
 &+\theta_1 S_{30}^* \left(\frac{S_{30}}{S_{30}^*} - \frac{S_{30}\mathcal{V}^*}{S_{30}^*\mathcal{V}} - \frac{\mathcal{V}}{\mathcal{V}^*} + 1 \right)
 \end{aligned}$$

$$\begin{aligned}
 & +\theta_2 S_{40}^* \left(\frac{S_{40}}{S_{40}^*} - \frac{S_{40} \mathcal{V}^*}{S_{40}^* \mathcal{V}^*} - \frac{\mathcal{V}}{\mathcal{V}^*} + 1 \right) \\
 & +\theta_3 S_{50}^* \left(\frac{S_{50}}{S_{50}^*} - \frac{S_{50} \mathcal{V}^*}{S_{50}^* \mathcal{V}^*} - \frac{\mathcal{V}}{\mathcal{V}^*} + 1 \right) \\
 & +\theta_4 S_{60}^* \left(\frac{S_{60}}{S_{60}^*} - \frac{S_{60} \mathcal{V}^*}{S_{60}^* \mathcal{V}^*} - \frac{\mathcal{V}}{\mathcal{V}^*} + 1 \right) \\
 & + (1 - \rho) \zeta \mathcal{Y}^* \mathcal{V}^* \left(\frac{\mathcal{V}}{\mathcal{V}^*} - \frac{\mathcal{Y} \mathcal{V}}{\mathcal{Y}^* \mathcal{V}^*} - \frac{\mathcal{Y}}{\mathcal{Y}^*} - 1 \right) \\
 & + \mathcal{Y}^* S_{30}^* \left(\frac{\mathcal{Y} S_{30}}{\mathcal{Y}^* S_{30}^*} - \frac{\mathcal{Y} S_{30} \mathcal{E}^*}{\mathcal{Y}^* S_{30}^* \mathcal{E}^*} - \frac{\mathcal{E}}{\mathcal{E}^*} + 1 \right) \\
 & + \mathcal{Y} \mathcal{Y}^* S_{40}^* \left(\frac{\mathcal{Y} S_{40}}{\mathcal{Y}^* S_{40}^*} - \frac{\mathcal{Y} S_{40} \mathcal{E}^*}{\mathcal{Y}^* S_{40}^* \mathcal{E}^*} - \frac{\mathcal{E}}{\mathcal{E}^*} + 1 \right) \\
 & + \delta \mathcal{Y}^* S_{50}^* \left(\frac{\mathcal{Y} S_{50}}{\mathcal{Y}^* S_{50}^*} - \frac{\mathcal{Y} S_{50} \mathcal{E}^*}{\mathcal{Y}^* S_{50}^* \mathcal{E}^*} - \frac{\mathcal{E}}{\mathcal{E}^*} + 1 \right) \\
 & + \zeta \mathcal{Y}^* S_{60}^* \left(\frac{\mathcal{Y} S_{60}}{\mathcal{Y}^* S_{60}^*} - \frac{\mathcal{Y} S_{60} \mathcal{E}^*}{\mathcal{Y}^* S_{60}^* \mathcal{E}^*} - \frac{\mathcal{E}}{\mathcal{E}^*} + 1 \right) \\
 & + (1 - \rho) \zeta \mathcal{Y}^* \mathcal{V}^* \left(\frac{\mathcal{Y} \mathcal{V}}{\mathcal{Y}^* \mathcal{V}^*} - \frac{\mathcal{Y} \mathcal{V} \mathcal{E}^*}{\mathcal{Y}^* \mathcal{V}^* \mathcal{E}^*} - \frac{\mathcal{E}}{\mathcal{E}^*} + 1 \right) \\
 & + \beta \varpi \mathcal{E}^* \left(\frac{2 \mathcal{E} \mathcal{E}^* I_1 I_1^* - \mathcal{E}^2 (I_1^*)^2 - (\mathcal{E}^*)^2 (I_1)^2}{\mathcal{E} \mathcal{E}^* I_1 I_1^*} \right) \\
 & + (1 - \beta) \varpi \mathcal{E}^* \left(\frac{2 \mathcal{E} \mathcal{E}^* I_{10} I_{10}^* - \mathcal{E}^2 (I_{10}^*)^2 - (\mathcal{E}^*)^2 (I_{10})^2}{\mathcal{E} \mathcal{E}^* I_{10} I_{10}^*} \right). \tag{42}
 \end{aligned}$$

In view of the arithmetic–geometric mean variant, which indicates that $d\mathcal{L}/d\xi \leq 0$. When $\mathbb{R}_0 > 1$, the argument $d\mathcal{L}/d\xi < 0$. The equality $d\mathcal{L}/d\xi = 0$ satisfies iff for $(S, S_{10}, S_{20}, S_{30}, S_{40}, S_{50}, S_{60}, \mathcal{V}, \mathcal{E}, I_1, I_{10}) = (S^*, S_{10}^*, S_{20}^*, S_{30}^*, S_{40}^*, S_{50}^*, S_{60}^*, \mathcal{V}^*, \mathcal{E}^*, I_1^*, I_{10}^*)$. Thus, the EE \bar{E}^* is GAS if $\mathbb{R}_0 > 1$. This completes the proof. \square

Existence and uniqueness

Here, we will use the f_p hypothesis and the Picard–Lindelöf technique on the model (11) to demonstrate the existence and uniqueness of the system (11) solution. To achieve this, we could reformat the framework in its following classic form:

$$\begin{cases}
 {}^c \Delta_0^\Psi \mathbf{X}(\xi) = \mathfrak{U}(\xi - 1 + \Psi, \mathbf{X}(\xi - 1 + \Psi)), \\
 \mathbf{X}(0) = \mathbf{X}_0,
 \end{cases} \tag{43}$$

where $\xi \in \tilde{\mathbb{N}}_{1-\Psi}^{\mathbb{T}^{\max}}$ in which $(\mathbb{T}^{\max} - 1 + \Psi) \in \tilde{\mathbb{N}}$, $\mathbf{X}(\xi) = (S(\xi), S_{10}(\xi), S_{20}(\xi), S_{30}(\xi), S_{40}(\xi), S_{50}(\xi), S_{60}(\xi), \mathcal{V}(\xi), \mathcal{E}(\xi), I_1(\xi), I_{10}(\xi), \mathcal{R}(\xi))^{\mathbb{T}}$ and the mapping $\mathfrak{U}(\xi, \mathbf{X}(\xi))$ is described as

$$\begin{cases}
 \mathfrak{U}_1(\xi, S) = \pi - (1 + \rho)S(\xi), \\
 \mathfrak{U}_2(\xi, S_{10}) = \ell S(\xi) - (1 + \rho)S_{10}(\xi), \\
 \mathfrak{U}_3(\xi, S_{20}) = (1 - \ell)S(\xi) - (1 + \rho)S_{20}(\xi), \\
 \mathfrak{U}_4(\xi, S_{30}) = \rho S_{10}(\xi) - (\mathcal{Y} + \theta_1 + \rho)S_{30}(\xi), \\
 \mathfrak{U}_5(\xi, S_{40}) = (1 - \nu)S_{10}(\xi) - \gamma \mathcal{Y} S_{40}(\xi) - (\theta_2 + \rho)S_{50}(\xi), \\
 \mathfrak{U}_6(\xi, S_{50}) = \sigma S_{20}(\xi) - \delta \mathcal{Y} S_{50}(\xi) - (\theta_3 + \rho)S_{50}(\xi), \\
 \mathfrak{U}_7(\xi, S_{60}) = (1 - \sigma)S_{20}(\xi) - \theta \mathcal{Y} S_{60}(\xi) - (\theta_4 + \rho)S_{60}(\xi), \\
 \mathfrak{U}_8(\xi, \mathcal{V}) = \theta_1 S_{30}(\xi) + \theta_2 S_{40}(\xi) + \theta_3 S_{50}(\xi) \\
 + \theta_4 S_{60}(\xi) - (1 - \rho) \zeta \mathcal{Y} \mathcal{V}(\xi) - (\rho + \rho) \mathcal{V}(\xi), \\
 \mathfrak{U}_9(\xi, \mathcal{E}) = \mathcal{Y} (S_{30}(\xi) + \gamma_2 S_{40}(\xi) + \delta S_{50}(\xi) + \theta S_{60}(\xi)) \\
 + (1 - \rho) \zeta \mathcal{Y} I_1(\xi) - (\varpi + \zeta + \rho) \mathcal{E}(\xi), \\
 \mathfrak{U}_{10}(\xi, I_1) = \beta \varpi \mathcal{E}(\xi) - (\eta_1 + \nu_1 + \rho) I_1(\xi), \\
 \mathfrak{U}_{11}(\xi, I_{10}) = (1 - \beta) \varpi \mathcal{E}(\xi) - (\eta_2 + \nu_2 + \rho) I_{10}(\xi), \\
 \mathfrak{U}_{12}(\xi, \mathcal{R}) = \rho \mathcal{V}(\xi) + \zeta \mathcal{E}(\xi) + \nu_1 I_1(\xi) + \nu_2 I_{10}(\xi) - \rho \mathcal{R}(\xi).
 \end{cases} \tag{44}$$

To conduct the E-U exploration, we use the IC $\mathbf{X}(0)$ and Proposition 1. It would immediately result in the following sum formulae for framework (11):

$$\begin{cases}
 S(\xi) - S(0) = \Delta_{1-\Psi}^{-\Psi} (\pi - (1 + \rho)S(\xi)), \\
 S_{10}(\xi) - S_{10}(0) = \Delta_{1-\Psi}^{-\Psi} (\ell S(\xi) - (1 + \rho)S_{10}(\xi)), \\
 S_{20}(\xi) - S_{20}(0) = \Delta_{1-\Psi}^{-\Psi} ((1 - \ell)S(\xi) - (1 + \rho)S_{20}(\xi)), \\
 S_{30}(\xi) - S_{30}(0) = \Delta_{1-\Psi}^{-\Psi} (\rho S_{10}(\xi) - (\mathcal{Y} + \theta_1 + \rho)S_{30}(\xi)), \\
 S_{40}(\xi) - S_{40}(0) = \Delta_{1-\Psi}^{-\Psi} ((1 - \nu)S_{10}(\xi) - \gamma \mathcal{Y} S_{40}(\xi) - (\theta_2 + \rho)S_{50}(\xi)), \\
 S_{50}(\xi) - S_{50}(0) = \Delta_{1-\Psi}^{-\Psi} (\sigma S_{20}(\xi) - \delta \mathcal{Y} S_{50}(\xi) - (\theta_3 + \rho)S_{50}(\xi)), \\
 S_{60}(\xi) - S_{60}(0) = \Delta_{1-\Psi}^{-\Psi} ((1 - \sigma)S_{20}(\xi) - \theta \mathcal{Y} S_{60}(\xi) - (\theta_4 + \rho)S_{60}(\xi)), \\
 \mathcal{V}(\xi) - \mathcal{V}(0) = \Delta_{1-\Psi}^{-\Psi} (\theta_1 S_{30}(\xi) + \theta_2 S_{40}(\xi) + \theta_3 S_{50}(\xi) \\
 + \theta_4 S_{60}(\xi) - (1 - \rho) \zeta \mathcal{Y} \mathcal{V}(\xi) - (\rho + \rho) \mathcal{V}(\xi)), \\
 \mathcal{E}(\xi) - \mathcal{E}(0) = \Delta_{1-\Psi}^{-\Psi} (\mathcal{Y} (S_{30}(\xi) + \gamma_2 S_{40}(\xi) + \delta S_{50}(\xi) + \theta S_{60}(\xi)) \\
 + (1 - \rho) \zeta \mathcal{Y} I_1(\xi) - (\varpi + \zeta + \rho) \mathcal{E}(\xi)), \\
 I_1(\xi) - I_1(0) = \Delta_{1-\Psi}^{-\Psi} (\beta \varpi \mathcal{E}(\xi) - (\eta_1 + \nu_1 + \rho) I_1(\xi)), \\
 I_{10}(\xi) - I_{10}(0) = \Delta_{1-\Psi}^{-\Psi} ((1 - \beta) \varpi \mathcal{E}(\xi) - (\eta_2 + \nu_2 + \rho) I_{10}(\xi)), \\
 \mathcal{R}(\xi) - \mathcal{R}(0) = \Delta_{1-\Psi}^{-\Psi} (\rho \mathcal{V}(\xi) + \zeta \mathcal{E}(\xi) + \nu_1 I_1(\xi) + \nu_2 I_{10}(\xi) - \rho \mathcal{R}(\xi)),
 \end{cases} \tag{45}$$

for $\xi \in \tilde{\mathbb{N}}_{1-\Psi}^{\mathbb{T}^{\max}}$. In view of (45) and Definition 1, we can find the state variables in contexts of $\mathfrak{U}_i(\xi, \mathbf{X}(\xi))$, where $i = 1, 2, \dots, 12$. Accordingly, we have

$$\begin{cases}
 S(\xi) = S(0) + \frac{1}{\Gamma(\Psi)} \sum_{\theta=1-\Psi}^{\xi-\Psi} (\xi - \theta - 1)^{(\Psi-1)} \mathfrak{U}_1 (\theta - 1 + \Psi, \\
 S(\theta - 1 + \Psi)), \\
 S_{10}(\xi) = S_{10}(0) + \frac{1}{\Gamma(\Psi)} \sum_{\theta=1-\Psi}^{\xi-\Psi} (\xi - \theta - 1)^{(\Psi-1)} \mathfrak{U}_2 (\theta - 1 + \Psi, \\
 S_{10}(\theta - 1 + \Psi)), \\
 S_{20}(\xi) = S_{20}(0) + \frac{1}{\Gamma(\Psi)} \sum_{\theta=1-\Psi}^{\xi-\Psi} (\xi - \theta - 1)^{(\Psi-1)} \mathfrak{U}_3 (\theta - 1 + \Psi, \\
 S_{20}(\theta - 1 + \Psi)), \\
 S_{30}(\xi) = S_{30}(0) + \frac{1}{\Gamma(\Psi)} \sum_{\theta=1-\Psi}^{\xi-\Psi} (\xi - \theta - 1)^{(\Psi-1)} \mathfrak{U}_4 (\theta - 1 + \Psi, \\
 S_{30}(\theta - 1 + \Psi)), \\
 S_{40}(\xi) = S_{40}(0) + \frac{1}{\Gamma(\Psi)} \sum_{\theta=1-\Psi}^{\xi-\Psi} (\xi - \theta - 1)^{(\Psi-1)} \mathfrak{U}_5 (\theta - 1 + \Psi, \\
 S_{40}(\theta - 1 + \Psi)), \\
 S_{50}(\xi) = S_{50}(0) + \frac{1}{\Gamma(\Psi)} \sum_{\theta=1-\Psi}^{\xi-\Psi} (\xi - \theta - 1)^{(\Psi-1)} \mathfrak{U}_6 (\theta - 1 + \Psi, \\
 S_{50}(\theta - 1 + \Psi)), \\
 S_{60}(\xi) = S_{60}(0) + \frac{1}{\Gamma(\Psi)} \sum_{\theta=1-\Psi}^{\xi-\Psi} (\xi - \theta - 1)^{(\Psi-1)} \mathfrak{U}_7 (\theta - 1 + \Psi, \\
 S_{60}(\theta - 1 + \Psi)), \\
 \mathcal{V}(\xi) = \mathcal{V}(0) + \frac{1}{\Gamma(\Psi)} \sum_{\theta=1-\Psi}^{\xi-\Psi} (\xi - \theta - 1)^{(\Psi-1)} \mathfrak{U}_8 (\theta - 1 + \Psi, \\
 \mathcal{V}(\theta - 1 + \Psi)), \\
 \mathcal{E}(\xi) = \mathcal{E}(0) + \frac{1}{\Gamma(\Psi)} \sum_{\theta=1-\Psi}^{\xi-\Psi} (\xi - \theta - 1)^{(\Psi-1)} \mathfrak{U}_9 (\theta - 1 + \Psi, \\
 \mathcal{E}(\theta - 1 + \Psi)), \\
 I_1(\xi) = I_1(0) + \frac{1}{\Gamma(\Psi)} \sum_{\theta=1-\Psi}^{\xi-\Psi} (\xi - \theta - 1)^{(\Psi-1)} \mathfrak{U}_{10} (\theta - 1 + \Psi, \\
 I_1(\theta - 1 + \Psi)), \\
 I_{10}(\xi) = I_{10}(0) + \frac{1}{\Gamma(\Psi)} \sum_{\theta=1-\Psi}^{\xi-\Psi} (\xi - \theta - 1)^{(\Psi-1)} \mathfrak{U}_{11} (\theta - 1 + \Psi, \\
 I_{10}(\theta - 1 + \Psi)), \\
 \mathcal{R}(\xi) = \mathcal{R}(0) + \frac{1}{\Gamma(\Psi)} \sum_{\theta=1-\Psi}^{\xi-\Psi} (\xi - \theta - 1)^{(\Psi-1)} \mathfrak{U}_{12} (\theta - 1 + \Psi, \\
 \mathcal{R}(\theta - 1 + \Psi)).
 \end{cases} \tag{46}$$

Consequently, we can arrive at the respective formulas using Picard iterations:

$$\begin{cases}
 S_{n+1}(\xi) = S(0) + \frac{1}{\Gamma(\Psi)} \sum_{\theta=1-\Psi}^{\xi-\Psi} (\xi - \theta - 1)^{(\Psi-1)} \mathfrak{U}_1 (\theta - 1 + \Psi, S(\theta - 1 + \Psi)), \\
 S_{10n+1}(\xi) = S_{10}(0) + \frac{1}{\Gamma(\Psi)} \sum_{\theta=1-\Psi}^{\xi-\Psi} (\xi - \theta - 1)^{(\Psi-1)} \mathfrak{U}_2 (\theta - 1 + \Psi, S_{10}(\theta - 1 + \Psi)), \\
 S_{20n+1}(\xi) = S_{20}(0) + \frac{1}{\Gamma(\Psi)} \sum_{\theta=1-\Psi}^{\xi-\Psi} (\xi - \theta - 1)^{(\Psi-1)} \mathfrak{U}_3 (\theta - 1 + \Psi, S_{20}(\theta - 1 + \Psi)), \\
 S_{30n+1}(\xi) = S_{30}(0) + \frac{1}{\Gamma(\Psi)} \sum_{\theta=1-\Psi}^{\xi-\Psi} (\xi - \theta - 1)^{(\Psi-1)} \mathfrak{U}_4 (\theta - 1 + \Psi, S_{30}(\theta - 1 + \Psi)), \\
 S_{40n+1}(\xi) = S_{40}(0) + \frac{1}{\Gamma(\Psi)} \sum_{\theta=1-\Psi}^{\xi-\Psi} (\xi - \theta - 1)^{(\Psi-1)} \mathfrak{U}_5 (\theta - 1 + \Psi, S_{40}(\theta - 1 + \Psi)), \\
 S_{50n+1}(\xi) = S_{50}(0) + \frac{1}{\Gamma(\Psi)} \sum_{\theta=1-\Psi}^{\xi-\Psi} (\xi - \theta - 1)^{(\Psi-1)} \mathfrak{U}_6 (\theta - 1 + \Psi, S_{50}(\theta - 1 + \Psi)), \\
 S_{60n+1}(\xi) = S_{60}(0) + \frac{1}{\Gamma(\Psi)} \sum_{\theta=1-\Psi}^{\xi-\Psi} (\xi - \theta - 1)^{(\Psi-1)} \mathfrak{U}_7 (\theta - 1 + \Psi, S_{60}(\theta - 1 + \Psi)), \\
 \mathcal{V}_{n+1}(\xi) = \mathcal{V}(0) + \frac{1}{\Gamma(\Psi)} \sum_{\theta=1-\Psi}^{\xi-\Psi} (\xi - \theta - 1)^{(\Psi-1)} \mathfrak{U}_8 (\theta - 1 + \Psi, \mathcal{V}(\theta - 1 + \Psi)), \\
 \mathcal{E}_{n+1}(\xi) = \mathcal{E}(0) + \frac{1}{\Gamma(\Psi)} \sum_{\theta=1-\Psi}^{\xi-\Psi} (\xi - \theta - 1)^{(\Psi-1)} \mathfrak{U}_9 (\theta - 1 + \Psi, \mathcal{E}(\theta - 1 + \Psi)), \\
 I_{1n+1}(\xi) = I_1(0) + \frac{1}{\Gamma(\Psi)} \sum_{\theta=1-\Psi}^{\xi-\Psi} (\xi - \theta - 1)^{(\Psi-1)} \mathfrak{U}_{10} (\theta - 1 + \Psi, I_1(\theta - 1 + \Psi)), \\
 I_{10n+1}(\xi) = I_{10}(0) + \frac{1}{\Gamma(\Psi)} \sum_{\theta=1-\Psi}^{\xi-\Psi} (\xi - \theta - 1)^{(\Psi-1)} \mathfrak{U}_{11} (\theta - 1 + \Psi, I_{10}(\theta - 1 + \Psi)), \\
 \mathcal{R}_{n+1}(\xi) = \mathcal{R}(0) + \frac{1}{\Gamma(\Psi)} \sum_{\theta=1-\Psi}^{\xi-\Psi} (\xi - \theta - 1)^{(\Psi-1)} \mathfrak{U}_{12} (\theta - 1 + \Psi, \mathcal{R}(\theta - 1 + \Psi)).
 \end{cases} \tag{47}$$

Accordingly, we can construct the preceding sum formula from framework (45) and its IC:

$$\mathbf{X}(\xi) = \mathbf{X}(0) + \frac{1}{\Gamma(\Psi)} \sum_{\theta=1-\Psi}^{\xi-\Psi} (\xi - \theta - 1)^{(\Psi-1)} \mathfrak{U}(\theta - 1 + \Psi, \mathbf{X}(\theta - 1 + \Psi)), \tag{48}$$

where $\xi \in \tilde{\mathbb{N}}_1$. The subsequent mathematical conclusions about the E-U of a solution for the present structure can be deduced as a consequence of the earlier research.

Lemma 3. The mapping $\mathfrak{U}(\xi, \mathbf{X}(\xi))$ stated in (44) holds the subsequent Lipschitz assumption:

$$\left| \mathfrak{U}(\xi, \mathbf{X}(\xi)) - \mathfrak{U}(\xi, \mathbf{X}^*(\xi)) \right| \leq \Xi \left\| \mathbf{X}(\xi) - \mathbf{X}^*(\xi) \right\|, \tag{49}$$

where

$$\Xi = \max \left\{ \begin{aligned}
 &\|1 + \rho\|, \|1 + \rho\|, \|1 + \rho\|, \|Y + \vartheta_1 + \rho\|, \|\gamma Y + \vartheta_2 + \rho\|, \\
 &\|\delta Y + \vartheta_3 + \rho\|, \|\theta Y + \vartheta_4 + \rho\|, \\
 &\|(1 - \rho)\zeta Y + (\rho + \rho)\|, \|(\varpi + \zeta + \rho)\|, \|\eta_1 + v_1 + \rho\|, \\
 &\|\eta_2 + v_2 + \rho\|, \|\rho\|.
 \end{aligned} \right. \tag{50}$$

Proof. By surmising $S(\xi)$ and $S^*(\xi)$ as two coupled mappings, we find

$$\left\| \mathfrak{U}_1(\xi, S) - \mathfrak{U}_1(\xi, S^*) \right\| = \left\| (1 + \rho)(S - S^*) \right\|. \tag{51}$$

In addition time, by considering

$$\Xi_1 = \left\| (1 + \rho) \right\|, \tag{52}$$

arrive at

$$\left\| \mathfrak{U}_1(\xi, S) - \mathfrak{U}_1(\xi, S^*) \right\| \leq \Xi_1 \left\| S - S^* \right\|. \tag{53}$$

The identical process leads to the following variants:

$$\begin{cases}
 \left\| \mathfrak{U}_2(\xi, S_{10}) - \mathfrak{U}_2(\xi, S_{10}^*) \right\| \leq \Xi_2 \left\| S_{10} - S_{10}^* \right\|, \\
 \left\| \mathfrak{U}_3(\xi, S_{20}) - \mathfrak{U}_3(\xi, S_{20}^*) \right\| \leq \Xi_3 \left\| S_{20} - S_{20}^* \right\|, \\
 \left\| \mathfrak{U}_4(\xi, S_{30}) - \mathfrak{U}_4(\xi, S_{30}^*) \right\| \leq \Xi_4 \left\| S_{30} - S_{30}^* \right\|, \\
 \left\| \mathfrak{U}_5(\xi, S_{40}) - \mathfrak{U}_5(\xi, S_{40}^*) \right\| \leq \Xi_5 \left\| S_{40} - S_{40}^* \right\|, \\
 \left\| \mathfrak{U}_6(\xi, S_{50}) - \mathfrak{U}_6(\xi, S_{50}^*) \right\| \leq \Xi_6 \left\| S_{50} - S_{50}^* \right\|, \\
 \left\| \mathfrak{U}_7(\xi, S_{60}) - \mathfrak{U}_7(\xi, S_{60}^*) \right\| \leq \Xi_7 \left\| S_{60} - S_{60}^* \right\|, \\
 \left\| \mathfrak{U}_8(\xi, \mathcal{V}) - \mathfrak{U}_8(\xi, \mathcal{V}^*) \right\| \leq \Xi_8 \left\| \mathcal{V} - \mathcal{V}^* \right\|, \\
 \left\| \mathfrak{U}_9(\xi, \mathcal{E}) - \mathfrak{U}_9(\xi, \mathcal{E}^*) \right\| \leq \Xi_9 \left\| \mathcal{E} - \mathcal{E}^* \right\|, \\
 \left\| \mathfrak{U}_{10}(\xi, I_1) - \mathfrak{U}_{10}(\xi, I_1^*) \right\| \leq \Xi_{10} \left\| I_1 - I_1^* \right\|, \\
 \left\| \mathfrak{U}_{11}(\xi, I_{10}) - \mathfrak{U}_{11}(\xi, I_{10}^*) \right\| \leq \Xi_{11} \left\| I_{10} - I_{10}^* \right\|, \\
 \left\| \mathfrak{U}_{12}(\xi, \mathcal{R}) - \mathfrak{U}_{12}(\xi, \mathcal{R}^*) \right\| \leq \Xi_{12} \left\| \mathcal{R} - \mathcal{R}^* \right\|,
 \end{cases} \tag{54}$$

where $\Xi_2 = \|1 + \rho\|$, $\Xi_3 = \|1 + \rho\|$, $\Xi_4 = \|Y + \vartheta_1 + \rho\|$, $\Xi_5 = \|\gamma Y + \vartheta_2 + \rho\|$, $\Xi_6 = \|\delta Y + \vartheta_3 + \rho\|$, $\Xi_7 = \|\theta Y + \vartheta_4 + \rho\|$, $\Xi_8 = \|(1 - \rho)\zeta Y + (\rho + \rho)\|$, $\Xi_9 = \|(\varpi + \zeta + \rho)\|$, $\Xi_{10} = \|\eta_1 + v_1 + \rho\|$, $\Xi_{11} = \|\eta_2 + v_2 + \rho\|$, $\Xi_{12} = \|\rho\|$.

From the aforesaid criteria, we can verify that the Lipschitz requirement is fulfilled by kernels \mathfrak{U}_i , $i = 1, 2, \dots, 12$. Also, if $\Xi_i < 1$, then kernel \mathfrak{U}_i is a contraction for $i = 1, \dots, 12$. \square

Theorem 5. Surmise that assumption (49) is fulfilled, then \exists a unique solution of the model (11) if

$$\frac{(\mathbb{T}_{\max} - 1 + \Psi)^{(\Psi)}}{\Gamma(\Psi + 1)} \Xi < 1. \tag{55}$$

Proof. In fact, the solution of the framework (11) can be described as

$$\mathbf{X}(\xi) = P_1(\mathbf{X}(\xi)), \tag{56}$$

where P_1 signifies the Picard operator stated by:

$$P_1(\mathbf{X}(\xi)) = \mathbf{X}(0) + \frac{1}{\Gamma(\Psi)} \sum_{\theta=1-\Psi}^{\xi-\Psi} (\xi - \theta - 1)^{(\Psi-1)} \mathfrak{U}(\theta - 1 + \Psi, \mathbf{X}(\theta - 1 + \Psi)). \tag{57}$$

Considering the preceding justifications, we can write

$$\left\| P_1(\mathbf{X}_1(\xi)) - P_1(\mathbf{X}_2(\xi)) \right\| = \left\| \frac{1}{\Gamma(\Psi)} \sum_{\theta=1-\Psi}^{\xi-\Psi} (\xi - \theta - 1)^{(\Psi-1)} \left(\mathfrak{U}(\theta - 1 + \Psi, \mathbf{X}_1(\theta - 1 + \Psi)) - \mathfrak{U}(\theta - 1 + \Psi, \mathbf{X}_2(\theta - 1 + \Psi)) \right) \right\|$$

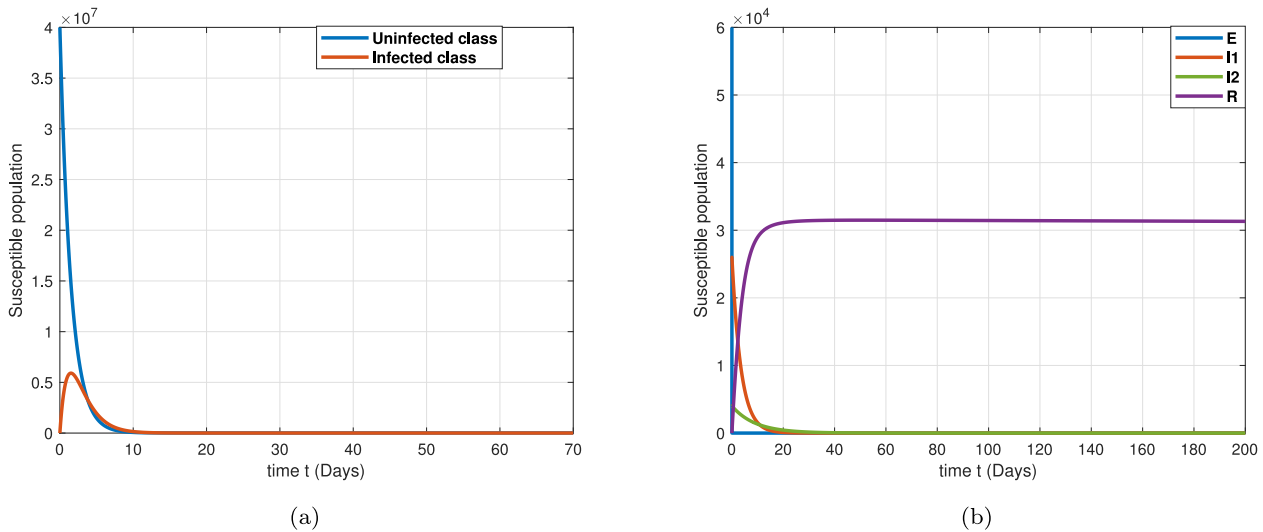


Fig. 5. Graphical view of the fractional-order model (11) (a) uninfected and infected class (b) time dependent graph for various compartments.

$$\begin{aligned}
 &\leq \frac{1}{\Gamma(\Psi)} \sum_{\theta=1-\Psi}^{\xi-\Psi} (\xi - \theta - 1)^{(\Psi-1)} \left\| \mathfrak{U}(\theta - 1 + \Psi, \right. \\
 &\mathbf{X}_1(\theta - 1 + \Psi)) \\
 &\quad \left. - \mathfrak{U}(\theta - 1 + \Psi, \mathbf{X}_2(\theta - 1 + \Psi)) \right\| \\
 &\leq \frac{1}{\Gamma(\Psi)} \sum_{\theta=1-\Psi}^{\xi-\Psi} (\xi - \theta - 1)^{(\Psi-1)} \max_{\theta \in \mathbb{N}_{1-\Psi}^{\xi-\Psi}} \left\| \mathfrak{U}(\theta - 1 \right. \\
 &+ \Psi, \mathbf{X}_1(\theta - 1 + \Psi)) \\
 &\quad \left. - \mathfrak{U}(\theta - 1 + \Psi, \mathbf{X}_2(\theta - 1 + \Psi)) \right\| \\
 &\leq \frac{(\mathbb{T}_{\max} - 1 + \Psi)^{(\Psi)}}{\Gamma(\Psi + 1)} \mathfrak{E} \left\| \mathbf{X}_1(\xi) - \mathbf{X}_2(\xi) \right\|. \quad (58)
 \end{aligned}$$

As $\frac{(\mathbb{T}_{\max} - 1 + \Psi)^{(\Psi)}}{\Gamma(\Psi + 1)} \mathfrak{E} < 1$, then the operator P_1 is contraction, where $\mathbb{T}_{\max} \geq \xi$. Therefore, model (11) has a unique solution. \square

Implementation to estimating COVID-19 behavior

To validate the conclusions drawn in the preceding sections, we will run a number of simulation studies in this portion. We will use our research for this purpose to forecast how the infection will behave in Thailand. We shall use a million-person sample size, which also implies we shall use 273523621 as the initial total population $\mathcal{N}(0)$. Thus according [64], it is simple to determine that the mortality rate is 0.4 and that there are $7.8277886e-5$ innovative births per day for every million people. The statistics can also be found on the website [64,65].

According to [49], we have performed numerical computations with different criteria and various time preferences, and in all scenarios, we have found a distinguishable solution. Table 1 contains an overview of the parameter estimation, information and value systems used in our simulation analysis. We determined the initial infectious disease number to compartment using the information obtained in Thailand as $S(0) = 40,000,000$, $S_{10}(0) = 0$, $S_{20}(0) = 0$, $S_{30}(0) = 0$, $S_{40}(0) = 0$, $S_{50}(0) = 0$, $S_{60}(0) = 0$, $\mathcal{V}(0) = 0$, $\mathcal{E}(0) = 60,000$, $I_1(0) = 26,000$, $I_{10}(0) = 4,000$ and $\mathcal{R}(0) = 0$ and the whole time span is $\mathbb{T} = 200$.

Eq. (24) requires that we first determine the fundamental reproduction number:

$$\begin{aligned}
 \mathbb{R}_0 &= \left\{ \begin{aligned} &\frac{\rho \ell (\rho + \theta + \theta_1 (1 - \rho) \zeta)}{(\rho + \theta)(\rho + \theta_1)(1 + \rho)^2} + \frac{(1 - \nu) \ell \pi (\gamma (\rho + \theta) + \theta_2 (1 - \rho) \zeta)}{(\rho + \theta)(\rho + \theta_2)(1 + \rho)^2} \\ &+ \frac{\sigma (1 - \ell) \pi (\delta (\rho + \theta) + \theta_3 (1 - \rho) \zeta)}{(\rho + \theta)(\rho + \theta_3)(1 + \rho)^2} + \frac{(1 - \sigma) (1 - \ell) \pi (\theta (\rho + \theta) + \theta_4 (1 - \rho) \zeta)}{(\rho + \theta)(\rho + \theta_4)(1 + \rho)^2} \\ &+ \frac{(v_2 + \eta_2 + \rho) (\wp_1 (v_1 + \eta_1 + \rho) + \wp_2 \Psi \varpi) + \wp_3 \varpi (1 - \Psi)(\rho + v_1 + \eta_1)}{(\rho + v_1 + \eta_1)(\rho + v_2 + \eta_2)(\rho + \varpi + \zeta)} \end{aligned} \right\} \\
 &= 0.567819 < 1,
 \end{aligned}$$

Mentioning that the DFE point is locally asymptotically stable, the requirements of (24) are satisfied. However, using these, we plot Figs. 5 and 6, which show simulation studies and demonstrate the framework (11) is reliable.

Use the incommensurate order system to get a prediction accuracy of as

$$\begin{cases}
 {}^c \Delta_0^{\Psi_1} S(\xi + 1 - \Psi) = \pi - (1 + \rho)S(\xi), \\
 {}^c \Delta_0^{\Psi_2} S_{10}(\xi + 1 - \Psi) = \ell S(\xi) - (1 + \rho)S_{10}(\xi), \\
 {}^c \Delta_0^{\Psi_3} S_{20}(\xi + 1 - \Psi) = (1 - \ell)S(\xi) - (1 + \rho)S_{20}(\xi), \\
 {}^c \Delta_0^{\Psi_4} S_{30}(\xi + 1 - \Psi) = \rho S_{10}(\xi) - (\gamma + \theta_1 + \rho)S_{30}(\xi), \\
 {}^c \Delta_0^{\Psi_5} S_{40}(\xi + 1 - \Psi) = (1 - \nu)S_{10}(\xi) - \gamma Y S_{40}(\xi) - (\theta_2 + \rho)S_{50}(\xi), \\
 {}^c \Delta_0^{\Psi_6} S_{50}(\xi + 1 - \Psi) = \sigma S_{20}(\xi) - \delta Y S_{50}(\xi) - (\theta_3 + \rho)S_{50}(\xi), \\
 {}^c \Delta_0^{\Psi_7} S_{60}(\xi + 1 - \Psi) = (1 - \sigma)S_{20}(\xi) - \theta Y S_{60}(\xi) - (\theta_4 + \rho)S_{60}(\xi), \\
 {}^c \Delta_0^{\Psi_8} \mathcal{V}(\xi + 1 - \Psi) = \theta_1 S_{30}(\xi) + \theta_2 S_{40}(\xi) + \theta_3 S_{50}(\xi) + \theta_4 S_{60}(\xi) \\
 \quad - (1 - \rho)\zeta Y \mathcal{V}(\xi) - (\rho + \rho)\mathcal{V}(\xi), \\
 {}^c \Delta_0^{\Psi_9} \mathcal{E}(\xi + 1 - \Psi) = Y(S_{30}(\xi) + \gamma_2 S_{40}(\xi) + \delta S_{50}(\xi) + \theta S_{60}(\xi)) \\
 \quad + (1 - \rho)\zeta Y \mathcal{V}(\xi) - (\varpi + \zeta + \rho)\mathcal{E}(\xi), \\
 {}^c \Delta_0^{\Psi_{10}} I_1(\xi + 1 - \Psi) = \beta \varpi \mathcal{E}(\xi) - (\eta_1 + v_1 + \rho)I_1(\xi), \\
 {}^c \Delta_0^{\Psi_{11}} I_{10}(\xi + 1 - \Psi) = (1 - \beta)\varpi \mathcal{E}(\xi) - (\eta_2 + v_2 + \rho)I_{10}(\xi), \\
 {}^c \Delta_0^{\Psi_{12}} \mathcal{R}(\xi + 1 - \Psi) = \rho \mathcal{V}(\xi) + \zeta \mathcal{E}(\xi) + v_1 I_1(\xi) + v_2 I_{10}(\xi) - \rho \mathcal{R}(\xi),
 \end{cases} \quad (59)$$

where $\Psi_i \in [0, 1]$, $i = 1, 2, \dots, 12$. Comparatively to defining a simple condition that interacts with the consistency of the interactions associated, it is challenging and possibly inconceivable in this scenario to create a straightforward and simple condition that interacts with the reliability of the system (59) in discussion (11). By identifying the significance of Ψ_i , $i = 1, 2, \dots, 12$, it is possible to examine the reliability of the \mathbf{f}_s s for framework (59) though. The following corollary must be reported in such a situation.

Corollary 1 ([59]). Assume that $\Psi_i \in (0, 1)$, $i = 1, 2, \dots, 12$, and \bar{M} is the least common multiple of \bar{u}_i and \bar{v}_i , hence, $\Psi_i = \frac{\bar{v}_i}{\bar{u}_i}$ having $\text{gcd}(\bar{u}_i, \bar{v}_i) = 1$ and $i = 1, 2, \dots, 12$, where $\text{gcd}(\dots)$ indicates the greatest common divisor. If one or more roots of the subsequent formulae:

$$\det \left(\text{diag} \left(\mathfrak{S}^{\bar{M}\Psi_1}, \mathfrak{S}^{\bar{M}\Psi_2}, \dots, \mathfrak{S}^{\bar{M}\Psi_{12}} \right) - (1 - \mathfrak{S}^{\bar{M}}) \mathbb{J} \right) = 0 \quad (60)$$

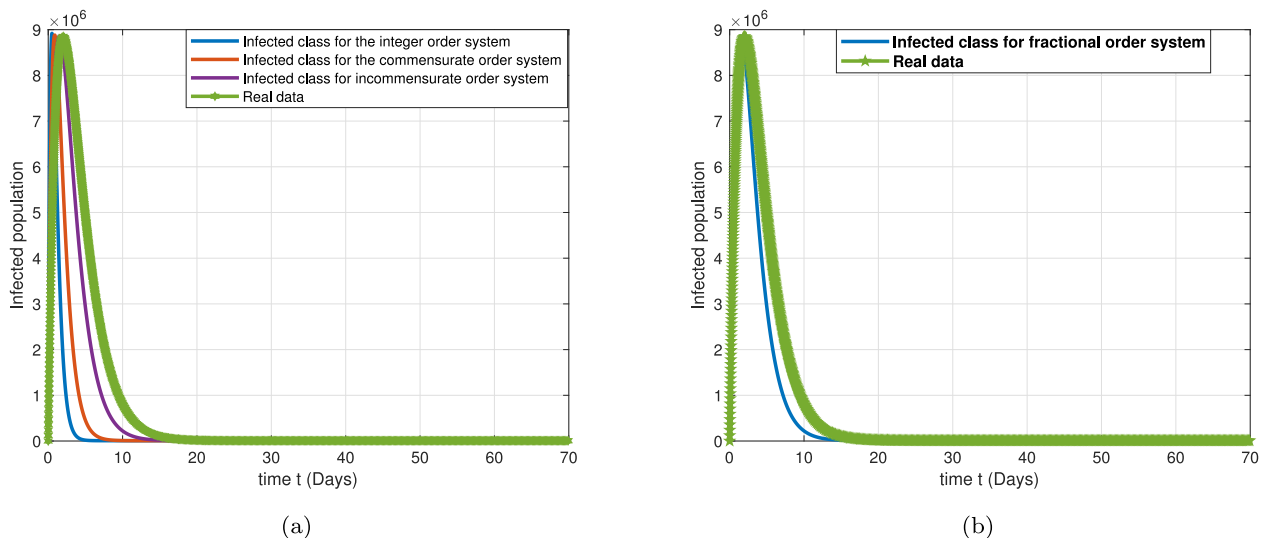


Fig. 6. Graphical view of the Covid-19 model (11) (a) the integer-order, the commensurate and the incommensurate order incorporating the real data (b) Time-dependent graph for the integer order and real data.

stays within the set $\mathbb{C} \setminus \mathcal{K}^{1/\bar{M}}$, then the trivial solution of model (59) respective to $(S(0), S_{10}(0), S_{20}(0), S_{30}(0), S_{40}(0), S_{50}(0), S_{60}(0), \mathcal{V}(0), \mathcal{E}(0), I_1(0), I_{10}(0), \mathcal{R}(0))$ is locally asymptotically stable, where

$$\mathcal{K}^{1/\bar{M}} = \left\{ \tilde{z} \in \mathbb{C} : |\tilde{z}| \leq (2 \cos(\bar{M} |\arg \tilde{z}|))^{1/\bar{M}} \text{ and } |\arg \tilde{z}| \leq \pi/2\bar{M} \right\}. \quad (61)$$

We will take into consideration that $\Psi_1 = 0.242, \Psi_2 = 0.243, \Psi_3 = 0.244, \Psi_4 = 0.245, \Psi_5 = 0.246, \Psi_6 = 0.247, \Psi_7 = 0.248, \Psi_8 = 0.249, \Psi_9 = 0.250, \Psi_{10} = 0.251, \Psi_{11} = 0.252, \Psi_{12} = 0.253$. When $\mathbb{R}_0 = 2.1126 > 1$, then the phase portrait for all initial exposed peoples is presented in Fig. 3. It is evident that every graph leads to an EE point. This modeling was functioning. We furthermore ran a test run for a longer time frame and the outcome was equivalent. Graphical view of (a) S vs. \mathcal{E} . (b) A comparison plot of \mathcal{E} and I . One of the crucial elements is vaccination, as shown in Fig. 4. Despite the fact that vaccines are only 50% efficacious, it is evident that immunization reduce can the number of pathogens. Additionally, given that they may hold the key to halting the disease’s propagation, our research suggests that at-risk individuals without any preventative measures be among the first in line for a comprehensive vaccination. It is significant to observe that the robust regulatory recommendations endorse vaccination at an elevated level of adherence for both high-risk and low-risk individuals who have not taken any measures to protect themselves from an ailment. Low-risk individuals who are attentive to safeguarding themselves, moreover, do not require any vaccination at all. The numerical simulations could be used to maintain vaccine transmission programs with constrained funding. Other precautions are still required because the illness can still infect those who have received the vaccine.

In contrast to the commensurate order situation, we get a more precise estimation in this illustration. A mathematical model (11) of this scenario is shown in Fig. 5, and comparisons between specific instances and factual facts are shown in Figs. 5 and 6, respectively. Fig. 6 also compares the integer order argument, the commensurate order specific instance, the incommensurate order example, and the factual facts. It is evident that the program gets quite precise with each application.

Conclusion

To capture the dynamics of COVID-19 in this study, a scheme of fractional difference equations was created. The population was segmented by the approach into those who adhere to preventive care

initiatives versus those who do not. The complexities of the framework that are free of infection and those that are prevalent were then examined. In specific, using the fundamental reproductive number \mathbb{R}_0 , we determined the local and global stability. With the aid of Picard Lindlöf approach, the existence-uniqueness of the solution for the suggested system have been examined. Several supportive mathematical conclusions have also been identified in illumination of the correlation between the predictability of the fixed points in this framework and the fundamental reproductive quantity. Numerous quantifiable modeling using MATLAB commands have been carried out to confirm such findings. In broad sense, we claim that the framework utilized in this research can be used to investigate the COVID-19 global epidemic in several parts of the globe, regardless of whether it is constructed using the fractional-order backward operator in either commensurate or incommensurate contexts.

Declaration of competing interest

The authors declare that they have no known competing financial interests or personal relationships that could have appeared to influence the work reported in this paper.

Data availability

No data was used for the research described in the article.

Acknowledgments

The researchers would like to acknowledge Deanship of Scientific Research, Taif University for funding this work.

References

- [1] Brauer F, Castillo-Chavez C, Feng Z. *Mathematical models in epidemiology*. New York: Springer-Verlag; 2019.
- [2] Ratnayake R, Finger F, Azman AS, Lantagne D, Funk S, Edmunds WJ, et al. Highly targeted spatiotemporal interventions against cholera epidemics, 2000–19: a scoping review. *Lancet Infect Dis* 2021;21:37–48.
- [3] Area I, Ndarrou F, Nieto JJ, Silva CJ, Torres DFM. Ebola model and optimal control with vaccination constraints. *J Ind Manag Optim* 2018;14:427–46.
- [4] Maayah B, Arqub OA, Alnabulsi S. Numerical solutions and geometric attractors of a fractional model of the cancer-immune based on the Atangana–Baleanu–Caputo derivative and the reproducing kernel scheme. *Chinese J Phys* 2022;80. <http://dx.doi.org/10.1016/j.cjph.2022.10.002>.

- [5] Silva CJ, Cruz C, Torres DFM, Munuzuri AP, Carballosa A, Area I, et al. Optimal control of the COVID-19 pandemic: controlled sanitary deconfinement in Portugal. *Sci Rep* 2021;11:3451.
- [6] Ndarrou F, Area I, Nieto JJ, Silva CJ, Torres DFM. Fractional model of COVID-19 applied to Galicia, Spain and Portugal. *Chaos Solitons Fractals* 2021;144:110652.
- [7] Kumar S, Chauhan RP, Momani S, Hadid S. Numerical investigations on COVID-19 model through singular and non-singular fractional operators. *Numer Methods Partial Differential Equations* 2020. <http://dx.doi.org/10.1002/num.22707>.
- [8] Lin YF, Duan Q, Zhou Y, et al. Spread and impact of COVID-19 in China: a systematic review and synthesis of predictions from transmission-dynamic models. *Front Med* 2020;7:321.
- [9] Giordano G, Blanchini F, Bruno R, Colaneri P, Di Filippo A, Di Matteo A, Colaneri M. Modeling the COVID-19 epidemic and implementation of population-wide interventions in Italy. *Nature Med* 2020;26:855–60.
- [10] Biala TA, Khaliq AQM. Fractional-order compartmental model for the spread of the COVID-19 pandemic. *Commun Nonlinear Sci Numer Simul* 2021;98:105764.
- [11] Oliveira JF, Jorge DC, Veiga RV, et al. Mathematical modeling of COVID-19 in 14.8 million individuals in Bahia, Brazil. *Nat Commun* 2021;12:333.
- [12] Peter OJ, Qureshi S, Yusuf A, Al-Shomrani M, Idowu AA. A new mathematical model of COVID-19 using real data from Pakistan. *Results Phys* 2021;24:104098.
- [13] Batiha IM, Momani S, Ouannas A, Momani Z, Hadid SB. Fractional-order COVID-19 pandemic outbreak: Modeling and stability analysis. *Int J Biomath* 2021;15:2150090.
- [14] Dwomoh D, Iddi S, Adu B, Aheto JM, Sedzro KM, Fobil J, et al. Mathematical modeling of COVID-19 infection dynamics in Ghana: impact evaluation of integrated government and individual level interventions. *Infect Dis Model* 2021;6:381–97.
- [15] Atangana A. A novel COVID-19 model with fractional differential operators with singular and non-singular kernels: analysis and numerical scheme based on Newton polynomial. *Alex Eng J* 2021;60:3781–806.
- [16] Kumar S, Kumar R, Momani S, Hadid S. A study on fractional COVID-19 disease model by using Hermite wavelets. *Math Methods Appl Sci* 2021. <http://dx.doi.org/10.1002/mma.7065>.
- [17] Safare KM, Betageri VS, Prakasha DG, Veerasha P, Kumar S. A mathematical analysis of ongoing outbreak COVID-19 in India through nonsingular derivative. *Numer Methods Partial Differential Equations* 2021;37:1282–98.
- [18] Hussain S, Madi EN, Khan H, Gulzar H, Etemad S, Rezapour S, et al. On the stochastic modeling of COVID-19 under the environmental white noise. *J Funct Spaces* 2022;2022:4320865.
- [19] Omay T, Baleanu D. Fractional unit-root tests allowing for a fractional frequency flexible Fourier form trend: predictability of COVID-19. *Adv Differential Equations* 2021;2021:167.
- [20] Zamir M, Nadeem F, Abdeljawad T, Hammouch Z. Threshold condition and non pharmaceutical interventions's control strategies for elimination of COVID-19. *Results Phys* 2021;20:103698.
- [21] El Koufi A, El Koufi N. Stochastic differential equation model of Covid-19: Case study of Pakistan. *Results Phys* 2022;34:105218.
- [22] Gao W, Baskonus HM, Shi L. New investigation of bats- hosts-reservoir-people coronavirus model and application to 2019-nCoV system. *Adv Differential Equations* 2020;2020:391.
- [23] CDC. Vaccines for COVID-19, centers for disease control and prevention. 2022, <https://www.cdc.gov/coronavirus/2019-ncov/vaccines/index.html>. [Accessed 21 January 2022].
- [24] Chu YM, Ali R, Asjad MI, Ahmadian M, Senu N. Heat transfer flow of Maxwell hybrid nanofluids due to pressure gradient into rectangular region. *Sci Rep* 2020;10:16643.
- [25] Rehman S, Mariam A, Ullah A, Asjad MI, Bajuri MY, Pansera BA, Ahmadian A. Numerical computation of buoyancy and radiation effects on MHD micropolar nanofluid flow over a stretching/shrinking sheet with heat source. *Case Stud Therm Eng* 2021;25:100867.
- [26] Çolakoğlu O, Kamran M, Bonyah E. M-polynomial and NM-polynomial of used drugs against monkeypox. *J Math* 2022;2022:9971255.
- [27] Rashid S, Ashraf R, Bonyah E. Nonlinear dynamics of the media addiction model using the fractal-fractional derivative technique. *Complexity* 2022;2022:1–13. <http://dx.doi.org/10.1155/2022/2140649>.
- [28] Ali R, Asjad MI, Aldalbahi A, Rahimi-Gorji M, Rahaman M. Convective flow of a Maxwell hybrid nanofluid due to pressure gradient in a channel. *J Therm Anal Calorim* 2021;143:1319–29.
- [29] Ali B, Ali L, Abdal S, Asjad MI. Significance of Brownian motion and thermophoresis influence on dynamics of Reiner–Rivlin fluid over a disk with non-Fourier heat flux theory and gyrotactic microorganisms: A numerical approach. *Phys Scr* 2021;96:094001. <http://dx.doi.org/10.1088/1402-4896/ac02f0>.
- [30] Rashid S, Kanwal B, Attique M, Bonyah E. An efficient technique for time-fractional water dynamics arising in physical systems pertaining to generalized fractional derivative operators. *Math Probl Eng* 2022;2022:6–25.
- [31] Rashid S, Butt SI, Hammouch Z, Bonyah E. An efficient method for solving fractional Black–Scholes model with index and exponential decay kernels. *J Funct Spaces* 2022;2022. <http://dx.doi.org/10.1155/2022/2613133>.
- [32] Mohammadi H, Rezapour S, Jajarmi A. On the fractional SIRD mathematical model and control for the transmission of COVID-19: the first and the second waves of the disease in Iran and Japan. *ISA Trans* 2021. <http://dx.doi.org/10.1016/j.isatra.2021.04.012>.
- [33] Baleanu D, Sajjadi SS, Jajarmi A, Deferli O, Asad JH. The fractional dynamics of a linear triatomic molecule. *Romanian Rep Phys* 2021;73:105.
- [34] Baleanu D, Sajjadi SS, Jajarmi A, Deferli O. On a nonlinear dynamical system with both chaotic and nonchaotic behaviors: a new fractional analysis and control. *Adv Differ Equ* 2021;2021:234.
- [35] Baleanu D, Sajjadi SS, Asad JH, Jajarmi A, Estiri E. Hyperchaotic behaviors, optimal control, and synchronization of a nonautonomous cardiac conduction system. *Adv Differ Equ* 2021;2021:157.
- [36] Baleanu D, Zibaei S, Namjoo M, Jajarmi A. A nonstandard finite difference scheme for the modeling and nonidentical synchronization of a novel fractional chaotic system. *Adv Differ Equ* 2021;2021:308.
- [37] Alqudah MA, Ravichandran C, Abdeljawad T, Valliammal N. New results on Caputo fractional-order neutral differential inclusions without compactness. *Adv Differ Equ* 2019;2019:528.
- [38] Ravichandran C, Trujillo JJ. Controllability of impulsive fractional functional integro-differential equations in Banach spaces. *J Funct Spaces* 2013;2013:812501.
- [39] Ravichandran C, Logeswari K, Jarad F. New results on existence in the framework of Atangana–Baleanu derivative for fractional integro-differential equations. *Chaos Solitons Fractals* 2019;125:194–200.
- [40] Wu G, Baleanu D. Discrete fractional logistic map and its chaos. *Nonlinear Dynam* 2014;75:283–7.
- [41] Wu G, Deng Z, Baleanu D, Zeng D. New variable-order fractional chaotic systems for fast image encryption. *Chaos* 2019;29:083103.
- [42] Bohner M, Peterson A. Dynamic equations on time scales: An introduction with applications. Boston: Birkhäuser; 2001.
- [43] Goodrich C, Peterson A. Discrete fractional calculus. Springer; 2015.
- [44] Atangana A, Goufo EFD. The Caputo–Fabrizio fractional derivative applied to a singular perturbation problem. *Int J Math Model Numer Optim* 2019;9:241–53.
- [45] Atangana A, Koca I. Model of thin viscous fluid sheet flow within the scope of fractional calculus: fractional derivative with and no singular kernel. *Fund Inform* 2017;151(1–4):145–59.
- [46] Atangana A. On the new fractional derivative and application to nonlinear Fisher's reaction–diffusion equation. *Appl Math Comput* 2016;273:948–56.
- [47] Atangana A, Alkahtani BST. Modeling the spread of rubella disease using the concept of with local derivative with fractional parameter: Beta-derivative. *Complex* 2016;21:442–51.
- [48] Atangana A. On the stability and convergence of the time-fractional variable order telegraph equation. *J Comput Phys* 2015;293:104–14.
- [49] Yong B, Hoseana J, Owen L. From pandemic to a new normal: Strategies to optimise governmental interventions in Indonesia based on an SVEIQHR-type mathematical model. *Infect Dis Model* 2022;7:346–63. <http://dx.doi.org/10.1016/j.idm.2022.06.004>.
- [50] Tang X, Musa SS, Zhao S, Mei S, He D. Using proper mean generation intervals in modeling of covid-19. *Front Public Health* 2021;9:691262.
- [51] Tang B, Wang X, Li Q, Bragazzi N, Tang S, Xiao Y, et al. Estimation of the transmission risk of the 2019-ncov and its implication for public health interventions. *J Clin Med* 2020;9. <http://dx.doi.org/10.3390/jcm9020462>.
- [52] Abioye AI, Peter OJ, Ogunseye HA, Oguntolu FA, Oshinubi K, Ibrahim AA, et al. Mathematical model of covid-19 in Nigeria with optimal control. *Res Phys* 2021;28:104598.
- [53] Choi W, Shim E. Optimal strategies for vaccination and social distancing in a game-theoretic epidemiologic model. *J Theor Biol* 2020;505:110422.
- [54] Adewole MO, Onifade AA, Abdullah FA, Kasali F, Ismailr AIM. Modeling the dynamics of covid-19 in Nigeria. *Int J Algorithms Comput Math* 2021;7:67.
- [55] Thongtha A, Modnak C. Optimal COVID-19 epidemic strategy with vaccination control and infection prevention measures in Thailand. *Infect Dis Model* 2022;7:835–55.
- [56] Abdeljawad T. On Riemann and Caputo fractional differences. *Comput Math Appl* 2011;62:1602–11.
- [57] Anastassiou GA. Discrete fractional calculus and inequalities. 2009, arXiv:0911.3370v1.
- [58] Lu Q, Zhu Y. Comparison theorems and distributions of solutions to uncertain fractional difference equations. *J Comput Appl Math* 2020;376:112884.
- [59] Shatnawi MT, Djenina N, Ouannas A, Batiha IM, Grassi G. Novel convenient conditions for the stability of nonlinear incommensurate fractional-order difference systems. *Alex Eng J* 2022;61:1655–63.
- [60] Cermák J, Györi I, Nechvátal L. On explicit stability conditions for a linear fractional difference system. *Fract Calc Appl Anal* 2015;18:651–72.
- [61] Van den Driessche P, Watmough J. Reproduction numbers and sub-threshold endemic equilibria for compartmental models of disease transmission. *Math Biosci* 2002;180:29–48.

- [62] Castillo-Chavez C, Huang ZFW. On computation of r_0 and its role on global stability. In: Mathematical approaches for emerging and reemerging infectious diseases: An introduction. IMA volumes in mathematics and its applications, Springer-Verlag; 2002.
- [63] LaSalle JP. The stability of dynamical systems. In: Regional conference series in applied mathematics. Philadelphia, PA, USA: SIAM; 1976.
- [64] WHO. Home/health topics/cardiovascular diseases, the world health organisation. 2022, <https://www.who.int/emergencies/diseases/novel-coronavirus-2019>. [Accessed 20 February 2022].
- [65] WHO. COVID-19 vaccines/COVID-19 vaccines advice, COVID-19 advice for the public: Getting vaccinated. 2021, <https://www.who.int/emergencies/diseases/novel-coronavirus-2019/covid-19-vaccines/advice>. [Accessed 24 November 2021].